PAPER

Ensemble Kalman inversion: a derivative-free technique for machine learning tasks

To cite this article: Nikola B Kovachki and Andrew M Stuart 2019 *Inverse Problems* **35** 095005

IOP Publishing Inverse Problems

Inverse Problems **35** (2019) 095005 (35pp) https://doi.org/10.1088/1361-6420/ab1c3a

Ensemble Kalman inversion: a derivative-free technique for machine learning tasks

Nikola B Kovachki and Andrew M Stuart

Computing and Mathematical Sciences, California Institute of Technology, Pasadena, CA 91125, United States of America

E-mail: nkovachki@caltech.edu and astuart@caltech.edu

Received 10 August 2018, revised 3 April 2019
Accepted for publication 24 April 2019
Published 20 August 2019

Abstract

The standard probabilistic perspective on machine learning gives rise to empirical risk-minimization tasks that are frequently solved by stochastic gradient descent (SGD) and variants thereof. We present a formulation of these tasks as classical inverse or filtering problems and, furthermore, we propose an efficient, gradient-free algorithm for finding a solution to these problems using ensemble Kalman inversion (EKI). The method is inherently parallelizable and is applicable to problems with non-differentiable loss functions, for which back-propagation is not possible. Applications of our approach include offline and online supervised learning with deep neural networks, as well as graph-based semi-supervised learning. The essence of the EKI procedure is an ensemble based approximate gradient descent in which derivatives are replaced by differences from within the ensemble. We suggest several modifications to the basic method, derived from empirically successful heuristics developed in the context of SGD. Numerical results demonstrate wide applicability and robustness of the proposed algorithm.

Keywords: machine learning, deep learning, derivative-free optimization, ensemble Kalman inversion, ensemble Kalman filtering

(Some figures may appear in colour only in the online journal)

1. Introduction

1.1. The setting

The field of machine learning has seen enormous advances over the last decade. These advances have been driven by two key elements: (i) the introduction of flexible architectures which have the expressive power needed to efficiently represent the input–output maps encountered in

practice; (ii) the development of smart optimization tools which train the free parameters in these input–output maps to match data. The text [22] overviews the start-of-the-art.

While there is little work in the field of derivative-free, paralellizable methods for machine learning tasks, such advancements are greatly needed. Variants on the Robbins–Monro algorithm [61], such as stochastic gradient descent (SGD), have become state-of-the-art for practitioners in machine learning [22] and an attendant theory [3, 15, 35, 46, 68] is emerging. However the approach faces many challenges and limitations [21, 58, 75]. New directions are needed to overcome them, especially for parallelization, as attempts to parallelize SGD have seen limited success [84].

A step in the direction of a derivative-free, parallelizable algorithm for the training of neural networks was attempted in [11] by use of the the method of auxiliary coordinates (MAC). Another approach using the alternating direction method of multipliers (ADMM) and a Bregman iteration is attempted in [75]. Both methods seem successful but are only demonstrated on supervised learning tasks with shallow, dense neural networks that have relatively few parameters. In reinforcement learning, genetic algorithm have seen some success (see [71] and references therein), but it is not clear how to deploy them outside of that domain.

To simultaneously address the issues of parallelizable and derivative-free optimization, we demonstrate in this paper the potential for using ensemble Kalman methods to undertake machine learning tasks. Optimizing neural networks via Kalman filtering has been attempted before (see [27] and references therein), but most have been through the use of extended or unscented Kalman filters. Such methods are plagued by inescapable computational and memory constraints and hence their application has been restricted to small parameter models. A contemporaneous paper by Haber *et al* [26] has introduced a variant on the ensemble Kalman filter, and applied it to the training of neural networks; our paper works with a more standard implementations of ensemble Kalman methods for filtering and inversion [34, 42] and demonstrates potential for these methods within a wide range of machine learning tasks, when suitably enhanced by ideas that have become routine in the successful implementation of SGD and its variants.

1.2. Our contribution

The goal of this work is two-fold:

- First we show that many of the common tasks considered in machine learning can be formulated in the unified framework of Bayesian inverse problems. The advantage of this point of view is that it allows for the transfer of theory and algorithms developed for inverse problems to the field of machine learning, in a manner accessible to the inverse problems community. To this end we give a precise, mathematical description of the most common approximation architecture in machine learning, the neural network (and its variants); we use the language of dynamical systems, and avoid references to the neurobiological language and notation more common-place in the applied machine learning literature. We do not pursue uncertainty quantification in this paper, but the framework in which we work will allow for this in the future. Work taking the deterministic viewpoint of inverse problems has already been pursued in [14].
- Secondly, adopting the inverse problem point of view, we show that variants of ensemble Kalman methods (EKI, EnKF) can be just as effective at solving most machine learning tasks as the plethora of gradient-based methods that are widespread in the field. We borrow some ideas from machine learning and optimization to modify these ensemble methods, to enhance their performance. In short we develop algorithms which do not

require backpropagation, but instead use an ensemble based approach to leverage sensitivities to perform parameter estimation; the method is inherently parallelizable.

Our belief is that by formulating machine learning tasks as inverse problems, and by demonstrating the potential for methodologies to be transferred from the field of inverse problems to machine learning, we will open up new ways of thinking about machine learning which may ultimately lead to deeper understanding of the optimization tasks at the heart of the field, and to improved methodology for addressing those tasks. To substantiate the second assertion we give examples of the competitive application of ensemble methods to supervised, semi-supervised, and online learning problems with deep dense, convolutional, and recurrent neural networks. To the best of our knowledge, this is the first paper to successfully apply ensemble Kalman methods to such a range of relatively large scale machine learning tasks. Furthermore we explicitly demonstrate that the method may be used on architectures for which backpropagation is not possible, for example in training a dense neural network with Heaviside activations on FashionMNIST. Whilst we do not attempt parallelization, ensemble methods are easily parallelizable and we give references to relevant literature. Our work leaves many open questions and future research directions for the inverse problems community.

1.3. Notation and overview

We adopt the notation $\mathbb{R}$ for the real axis, $\mathbb{R}_+$ the subset of non-negative reals, and $\mathbb{N} = \{0, 1, 2, \dots\}$ for the set of natural numbers. For any set A, we use A^n to denote its n-fold Cartesian product for any $n \in \mathbb{N} \setminus \{0\}$. For any function $f : A \to B$, we use $\mathrm{Im}(f) = \{y \in B : y = f(x), \text{for some } x \in A\}$ to denote its image. For any subset $V \subseteq \mathcal{X}$ of a linear space $\mathcal{X}$, we let $\dim V$ denote the dimension of the smallest subspace containing V. For any Hilbert space $\mathcal{H}$, we adopt the notation $\|\cdot\|_{\mathcal{H}}$ and $\langle\cdot,\cdot\rangle_{\mathcal{H}}$ to be its associated norm and inner-product respectively. Furthermore for any symmetric, positive-definite operator $C : \mathcal{D}(C) \subset \mathcal{H} \to \mathcal{H}$, we use the notation $\|\cdot\|_C = \|C^{-\frac{1}{2}}\cdot\|_{\mathcal{H}}$ and $\langle\cdot,\cdot\rangle_C = \langle C^{-\frac{1}{2}}\cdot, C^{-\frac{1}{2}}\cdot,\rangle_{\mathcal{H}}$. For any two topological spaces $\mathcal{X}, \mathcal{Y}$, we let $C(\mathcal{X}, \mathcal{Y})$ denote the set of continuous functions from $\mathcal{X}$ to $\mathcal{Y}$. We define

$$\mathbb{P}^m = \{y \in \mathbb{R}^m \mid \|y\|_1 = 1, y_1, \dots, y_m \geqslant 0\}$$

the set of m-dimensional probability vectors, and the subset

$$\mathbb{P}_0^m = \{y \in \mathbb{R}^m \mid \|y\|_1 = 1, y_1, \dots, y_m > 0\}.$$

Section 2 delineates the learning problem, starting from the classical, optimization-based framework, and shows how it can be formulated as a Bayesian inverse problem. Section 3 gives a brief overview of modern neural network architectures as dynamical systems. Section 4 outlines the state-of-the-art algorithms for fitting neural network models, as well as the EKI method and our proposed modifications of it. Section 5 presents our numerical experiments, comparing and contrasting EKI methods with the state-of-the-art. Section 6 gives some concluding remarks and possible future directions for this line of work.

2. Problem formulation

Section 2.1 overviews the standard formulation of machine learning problems with sections 2.1.1–2.1.3 presenting supervised, semi-supervised, and online learning respectively. Section 2.2 sets forth the Bayesian inverse problem interpretation of these tasks and gives examples for each of the previously presented problems.

2.1. Classical framework

The problem of supervised learning is usually formulated as minimizing an expected cost over some space of mappings relating the data [22, 51, 77]. More precisely, let $\mathcal{X}$, $\mathcal{Y}$ be separable Hilbert spaces and let $\mathbb{P}(x, y)$ be a probability measure on the product space $\mathcal{X} \times \mathcal{Y}$. Let $\mathcal{L} : \mathcal{Y} \times \mathcal{Y} \to \mathbb{R}_+$ be a positive-definite function and define $\mathcal{F}$ to be the set of mappings $\{\mathcal{G} : \mathcal{X} \to \mathcal{Y}\}$ on which the composition $\mathcal{L}(\mathcal{G}(\cdot), \cdot)$ is $\mathbb{P}$-measurable for all $\mathcal{G}$ in $\mathcal{F}$. Then we seek to minimize the functional

$$Q(\mathcal{G}) = \int_{\mathcal{X}\times\mathcal{Y}} \mathcal{L}(\mathcal{G}(x), y)\, \mathrm{d}\mathbb{P}(x, y) \tag{1}$$

across all mappings in $\mathcal{F}$. This minimization may not be well defined as there could be infimizing sequences not converging in $\mathcal{F}$. Thus further constraints (regularization) are needed to obtain an unambiguous optimization problem. These are generally introduced by working with parametric forms of $\mathcal{G}$. Additional, explicit regularization is also often added to parameterized versions of (1).

Usually $\mathcal{L}$ is called the loss or cost function and acts as a metric-like function on $\mathcal{Y}$; however it is useful in applications to relax the strict properties of a metric, and we, in particular, do not require $\mathcal{L}$ to be symmetric or subadditive. With this interpretation of $\mathcal{L}$ as a cost, we are seeking a mapping $\mathcal{G}$ with lowest cost, on average with respect to $\mathbb{P}$. There are numerous choices for $\mathcal{L}$ used in applications [22]; some of the most common include the squared-error loss $\mathcal{L}(y', y) = \|y - y'\|^2_{\mathcal{Y}}$ used for regression tasks, and the cross-entropy loss $\mathcal{L}(y', y) = -\langle y, \log y' \rangle_{\mathcal{Y}}$ used for classification tasks. In both these cases we often have $\mathcal{Y} = \mathbb{R}^K$, and, for classification, we may restrict the class of mappings to those taking values in $\mathbb{P}^K_0$.

Most of our focus will be on *parametric* learning where we approximate $\mathcal{F}$ by a parametric family of models $\{\mathcal{G}(u|\cdot) : \mathcal{X} \to \mathcal{Y}\}$ where $u \in \mathcal{U}$ is the parameter and $\mathcal{U}$ is a separable Hilbert space. This allows us to work with a computable class of functions and perform the minimization directly over $\mathcal{U}$. Much of the early work in machine learning focuses on model classes which make the associated minimization problem convex [9, 30, 51], but the recent empirical success of neural networks has driven research away from this direction [22, 43]. In section 3, we give a brief overview of the model space of neural networks.

While the formulation presented in (1) is very general, it is not directly transferable to practical applications as, typically, we have no direct access to $\mathbb{P}(x, y)$. How we choose to address this issue depends on the information known to us, usually in the form of a data set, and defines the type of learning. Typically information about $\mathbb{P}$ is accessible only through our sample data. The next three subsections describe particular structures of such sample data sets which arise in applications, and the minimization tasks which are constructed from them to determine the parameter u.

2.1.1. Supervised learning. Suppose that we have a dataset $\{(x_j, y_j)\}_{j=1}^N$ assumed to be i.i.d. samples from $\mathbb{P}(x, y)$. We can thus replace the integral (1) with its Monte Carlo approximation, and add a regularization term, to obtain the following minimization problem:

$$\arg\min_{u\in\mathcal{U}} \Phi_{\mathrm{s}}(u; \mathsf{x}, \mathsf{y}), \tag{2}$$

$$\Phi_{\mathrm{s}}(u; \mathsf{x}, \mathsf{y}) = \frac{1}{N}\sum_{j=1}^{N} \mathcal{L}(\mathcal{G}(u|x_j), y_j) + R(u). \tag{3}$$

Here $R : \mathcal{U} \to \mathbb{R}$ is a regularizer on the parameters designed to prevent overfitting or address possible ill-posedness. We use the notation $\mathsf{x} = [x_1, \dots, x_N] \in \mathcal{X}^N$, and analogously y, for concatenation of the data in the input and output spaces $\mathcal{X}, \mathcal{Y}$ respectively.

A common choice of regularizer is $R(u) = \lambda \|u\|_{\mathcal{U}}^2$ where $\lambda \in \mathbb{R}$ is a tunable parameter. This choice is often called *weight decay* in the machine learning literature; the regularizer promotes parameters with smaller norm, thus inducing decay when represented in specific bases. Other choices, such as sparsity promoting norms, are also employed; carefully selected choices of the norm can induce desired behavior in the parameters [10, 78]. We note also that Monte Carlo approximation is itself a form of regularization of the minimization task (1).

This formulation is known as *supervised* learning. Supervised learning is perhaps the most common type of machine learning with numerous applications including image/video classification, object detection, and natural language processing [41, 48, 73].

2.1.2. Semi-supervised learning. Suppose now that we only observe a small portion of the data y in the image space; specifically we assume that we have access to data $\{x_j\}_{j \in Z}$, $\{y_j\}_{j \in Z'}$ where $x_j \in \mathcal{X}, y_j \in \mathcal{Y}$, $Z = \{1, \dots, N\}$ and where $Z' \subset Z$ with $|Z'| \ll |Z|$. Clearly this can be turned into supervised learning by ignoring all data indexed by $Z \setminus Z'$, but we would like to take advantage of all the information known to us. Often the data in $\mathcal{X}$ is known as unlabeled data, and the data in $\mathcal{Y}$ as labeled data; in particular the labeled data is often in the form of categories. We use the terms labeled and unlabeled in general, regardless or whether the data in $\mathcal{Y}$ is categorical; however some of our illustrative discussion below will focus on the binary classification problem. The objective is to assign a label y_j to every $j \in Z$. This problem is known as *semi-supervised* learning.

One approach to the problem is to seek to minimize

$$\arg\min_{u \in \mathcal{U}} \Phi_{\mathrm{ss}}(u; \mathsf{x}, \mathsf{y}) \tag{4}$$

$$\Phi_{\mathrm{ss}}(u; \mathsf{x}, \mathsf{y}) = \frac{1}{|Z'|} \sum_{j \in Z'} \mathcal{L}(\mathcal{G}(u|x_j), y_j) + R(u; \mathsf{x}) \tag{5}$$

where the regularizer $R(u; \mathsf{x})$ may use the unlabeled data in $Z \backslash Z'$, but the loss term involves only labeled data in Z'.

There are a variety of ways in which one can construct the regularizer $R(u; \mathsf{x})$ including graph-based and low-density separation methods [6, 7]. In this work, we will study a nonparametric graph approach where we think of Z as indexing the nodes on a graph. To illustrate ideas we consider the case of binary outputs, take $\mathcal{Y} = \mathbb{R}$ and restrict attention to mappings $\mathcal{G}(u|\cdot)$ which take values in $\{-1, 1\}$; we sometimes abuse notation and simply take $\mathcal{Y} = \{-1, 1\}$, so that $\mathcal{Y}$ is no longer a Hilbert space. We assume that $\mathcal{U}$ comprises real-valued functions on the nodes Z of the graph, equivalently vectors in $\mathbb{R}^N$. We specify that $\mathcal{G}(u|j) = \mathrm{sgn}(u(j))$ for all $j \in Z$, and take, for example, the probit or logistic loss function [7, 60]. Once we have found an optimal parameter value for $u : Z \to \mathbb{R}$, application of $\mathcal{G}$ to u will return a labeling over all nodes j in Z. In order to use all the unlabeled data we introduce edge weights which measure affinities between nodes of a graph with vertices Z, by means of a weight function on $\mathcal{X} \times \mathcal{X}$. We then compute the graph Laplacian $\mathsf{L}(\mathsf{x})$ and use it to define a regularizer in the form

$$R(u; \mathsf{x}) = \langle u, (\mathsf{L}(\mathsf{x}) + \tau^2 I)^{\alpha} u \rangle_{\mathbb{R}^N}.$$

Here I is the identity operator, and $\tau, \alpha \in \mathbb{R}$ with $\alpha > 0$ are tunable parameters. Further details of this method are in the following section. Applications of semi-supervised learning

can include any situation where data in the image space $\mathcal{Y}$ is hard to come by, for example because it requires expert human labeling; a specific example is medical imaging [47].

2.1.3. Online learning. Our third and final class of learning problems concerns situations where samples of data are presented to us sequentially and we aim to refine our choice of parameters at each step. We thus have the supervised learning problem (2) and we aim to solve it sequentially as each pair of data points $\{x_j, y_j\}$ is delivered. To facilitate cheap algorithms we impose a Markovian structure in which we are allowed to use only the current data sample, as well as our previous estimate of the parameters, when searching for the new estimate. We look for a sequence $\{u_j\}_{j=1}^{\infty} \subset \mathcal{U}$ such that $u_j \to u^*$ as $j \to \infty$ where, in the perfect scenario, u^* will be a minimizer of the limiting learning problem (1). To make the problem Markovian, we may formulate it as the following minimization task

$$u_j = \arg\min_{u \in \mathcal{U}} \Phi_{\mathrm{o}}(u, u_{j-1}; x_j, y_j) \tag{6}$$

$$\Phi_{\mathrm{o}}(u, u_{j-1}; x_j, y_j) = \mathcal{L}(\mathcal{G}(u|x_j), y_j) + R(u; u_{j-1}) \tag{7}$$

where R is again a regularizer that could enforce a closeness condition between consecutive parameter estimates, such as

$$R(u; u_{j-1}) = \lambda \|u - u_{j-1}\|_{\mathcal{U}}^2.$$

Furthermore this regularization need not be this explicit, but could rather be included in the method chosen to solve (6). For example if we use an iterative method for the minimization, we could simply start the iteration at u_{j-1}.

This formulation of supervised learning is known as *online* learning. It can be viewed as reducing computational cost as a cheaper, sequential way of estimating a solution to (1); or it may be necessitated by the sequential manner in which data is acquired.

2.2. Inverse problems

The preceding discussion demonstrates that, while the goal of learning is to find a mapping which generalizes across the whole distribution of possible data, in practice, we are severely restricted by only having access to a finite data set. Namely formulations (2), (4) and (6) can be stated for any input–output pair data set with no reference to $\mathbb{P}(x, y)$ by simply assuming that there exists some function in our model class that will relate the two. In fact, since $\mathcal{L}$ is positive-definite, its dependence also washes out when ones takes a function approximation point of view.

To make the above precise, consider the inverse problem of finding $u \in \mathcal{U}$ such that

$$\mathsf{y} = \mathsf{G}(u|\mathsf{x}) + \eta; \tag{8}$$

here $\mathsf{G}(u|\mathsf{x}) = [\mathcal{G}(u|x_1), \ldots, \mathcal{G}(u|x_N)]$ is a concatenation and $\eta \sim \pi$ is a $\mathcal{Y}^N$-valued random variable distributed according to a measure π that models possible noise in the data, or model error. In order to facilitate a Bayesian formulation of this inverse problem we let μ_0 denote a prior probability measure on the parameters u. Then supposing

$$-\log(\pi(\mathsf{y} - \mathsf{G}(u|\mathsf{x}))) \propto \sum_{j=1}^{N} \mathcal{L}(\mathcal{G}(u|x_j), y_j)$$

$$-\log(\mu_0(u)) \propto R(u)$$

we see that (2) corresponds to the standard MAP estimator arising from a Bayesian formulation of (8). The semi-supervised learning problem (4) can also be viewed as a MAP estimator by restricting (8) to Z' and using x to build μ_0. This is the perspective we take in this work and we illustrate with an example for each type of problem.

Example 2.1. Suppose that $\mathcal{Y}$ and $\mathcal{U}$ are Euclidean spaces and let $\pi = \mathcal{N}(0, \Gamma)$ and $\mu_0 = \mathcal{N}(0, \Sigma)$ be Gaussian with positive-definite covariances Γ, Σ where Γ is block-diagonal with N identical blocks Γ_0. Computing the MAP estimator of (8), we obtain that $\mathcal{L}(y', y) = \|y - y'\|^2_{\Gamma_0}$ and $R(u) = \|u\|^2_\Sigma$.

Example 2.2. Suppose that $\mathcal{U} = \mathbb{R}^N$ and $\mathcal{Y} = \mathbb{R}$ with the data $y_j = \pm 1 \ \forall j \in Z'$. We will take the model class to be a single function $\mathcal{G} : \mathbb{R}^N \times Z \to \mathbb{R}$ depending only on the index of each data point and defined by $\mathcal{G}(u|j) = \operatorname{sgn}(u_j)$. As mentioned, we think of Z as the nodes on a graph and construct the edge set $E = (e_{ij}) = \eta(x_i, x_j)$ where $\eta : \mathcal{X} \times \mathcal{X} \to \mathbb{R}_+$ is a symmetric function. This allows construction of the associated graph Laplacian $\mathsf{L}(\mathsf{x})$. We shift it to remove its null space and consider powers of this operator leading to the symmetric, positive-definite operator $C = (\mathsf{L}(\mathsf{x}) + \tau^2 I)^{-\alpha}$ from which we can define the Gaussian measure $\mu_0 = \mathcal{N}(0, C)$. For details on why this construction defines a reasonable prior we refer to [7]. Letting $\pi = \mathcal{N}(0, \frac{1}{\gamma^2} I)$, we restrict (8) to the inverse problem

$$y_j = \mathcal{G}(u|j) + \eta_j \quad \forall j \in Z'.$$

With the given definitions, letting $\gamma^2 = |Z'|$, the associated MAP estimator has the form of (4), namely

$$\frac{1}{|Z'|} \sum_{j \in Z'} |\mathcal{G}(u|j) - y_j|^2 + \langle u, C^{-1} u \rangle_{\mathbb{R}^N}.$$

The infimum for this functional is not achieved [33], but the ensemble based methods we employ to solve the problem implicitly apply a further regularization which circumvents this issue.

Example 2.3. Lastly we turn to the online learning problem (6). We assume that there is some unobserved, fixed in time parameter of our model that will perfectly match the observed data up to a noise term. Our goal is to estimate this parameter sequentially. Namely, we consider the stochastic dynamical system,

$$\begin{aligned} u_{j+1} &= u_j \\ y_{j+1} &= \mathcal{G}(u_{j+1}|x_{j+1}) + \eta_{j+1} \end{aligned} \tag{9}$$

where the sequence $\{\eta_j\}$ are $\mathcal{Y}$-valued i.i.d. random variables that are also independent from the data. This is an instance of the classic filtering problem considered in data assimilation [42]. We may view this as solving an inverse problem at each fixed time with increasingly strong prior information as time unrolls. With the appropriate assumptions on the prior and the noise model, we may again view (6) as the MAP estimators of each fixed inverse problem. Thus we may consider all problems presented here in the general framework of (8).

3. Approximation architectures

In this section, we outline the approximation architectures that we will use to solve the three machine learning tasks outlined in the preceding section. For supervised and online learning

these amount to specifying the dependence of $\mathcal{G}$ on u; for semi-supervised learning this corresponds to determining a basis in which to seek the parameter u. We do not give further details for the semi-supervised case as our numerics fit in the context of example 2.2, but we refer the reader to [7] for a detailed discussion.

Section 3.1 details feed-forward neural networks with sections 3.1.1 and 3.1.2 showing the parameterizations of dense and convolutional networks respectively.

3.1. Feed-forward neural networks

Feed-forward neural networks are a parametric model class defined as discrete time, nonautonomous, semi-dynamical systems of an unusual type. Each map in the composition takes a specific parametrization and can change the dimension of its input while the whole system is computed only up to a fixed time horizon. To make this precise, we will assume $\mathcal{X} = \mathbb{R}^d$, $\mathcal{Y} = \mathbb{R}^m$ and define a neural network with $n \in \mathbb{N}$ hidden layers as the composition

$$\mathcal{G}(u|x) = (S \circ A \circ F_{n-1} \circ \cdots \circ F_0)(x)$$

where $d_0 = d$ and $F_j \in C(\mathbb{R}^{d_j}, \mathbb{R}^{d_{j+1}}), n = 0, \ldots, n-1$ are nonlinear maps, referred to as *layers*, depending on parameters $\theta_0, \ldots, \theta_{n-1}$ respectively, $A : \mathbb{R}^{d_n} \to \mathbb{R}^m$ is an affine map with parameters θ_n, and $u = [\theta_0, \ldots, \theta_n]$ is a concatenation. The map $S : \mathbb{R}^m \to V \subseteq \mathbb{R}^m$ is fixed and thought of as a projection or thresholding done to move the output to the appropriate subset of data space. The choice of S is dependent on the problem at hand. If we are considering a regression task and $V = \mathbb{R}^m$ then S can simply be taken as the identity. On the other hand, if we are considering a classification task and $V = \mathbb{P}^m$, the set of probability vectors in $\mathbb{R}^m$, then S is often taken to be the softmax function defined as

$$S(w) = \frac{1}{\sum_{j=1}^m \mathrm{e}^{w_j}} (\mathrm{e}^{w_1}, \ldots, \mathrm{e}^{w_m}).$$

From this perspective, the neural network approximates a categorical distribution of the input data and the softmax arises naturally as the canonical response function of the categorical distribution (when viewed as belonging to the exponential family of distributions) [49, 64]. If we have some specific bounds for the output data, for example $V = [-1, 1]^m$ then S can be a point-wise hyperbolic tangent.

3.1.1. Dense networks. A key feature of neural networks is the specific parametrization of each map F_k. In the most basic case, each F_k is an affine map followed by a point-wise nonlinearity, in particular,

$$F_k(z_k) = \sigma(W_k z_k + b_k)$$

where $W_k \in \mathbb{R}^{d_{k+1} \times d_k}$, $b_k \in \mathbb{R}^{d_{k+1}}$ are the parameters i.e. $\theta_k = [W_k, b_k]$ and $\sigma \in C(\mathbb{R}, \mathbb{R})$ is non-constant and bounded; we extend σ to a function on $\mathbb{R}^d$ by defining it point-wise as $\sigma(u)_j = \sigma(u_j)$ for any vector $u \in \mathbb{R}^d$. This layer type is referred to as *dense*, or fully-connected, because each entry in W_k is a parameter with no global sparsity assumptions and hence we can end up with a dense matrix. A neural network with only this type of layer is called dense or fully-connected (DNN).

The nonlinearity σ, called the *activation function*, is a design choice and usually does not vary from layer to layer. Some popular choices include the sigmoid, the hyperbolic tangent, or the rectified linear unit (ReLU) defined by $\sigma(q) = \max\{0, q\}$. Note that ReLU is unbounded and hence does not satisfy the assumptions for the classical universal approximation theorem

[31], but it has shown tremendous numerical success when the associated inverse problem is solved via backpropagation (method of adjoints) [53].

3.1.2. Convolutional networks. Instead of seeking the full representation of a linear operator at each time step, we may consider looking only for the parameters associated to a pre-specified type of operator. Namely we consider

$$F_k(z_k) = \sigma(W(s_k)z_k + b_k)$$

where W can be fully specified by the parameter s_k. The most commonly considered operator is the one arising from a discrete convolution [44]. The motivation behind this choice lies in the application to natural images where we want to exploit spatial features of the data. In particular, considering objects in an image, a natural choice is to pick a transformation which is translation equivariant. Namely, translations in the image result in equivalent translations in the output. This captures the property that moving an object in an image does not change the content of that image. Convolution then becomes the natural choice as as the set of convolutions is in bijection with the set of equivariant functions.

We consider the input z_k as a function on the integers with period d_k then we may define $W(s_k)$ as the circulant matrix arising as the kernel of the discrete circular convolution with convolution operator s_k. Exact construction of the operator W is a modeling choice as one can pick exactly which blocks of z_k to compute the convolution over. Usually, even with maximally overlapping blocks, the operation is dimension reducing, but can be made dimension preserving, or even expanding, by appending zero entries to z_k. This is called *padding*. For brevity, we omit exact descriptions of such details and refer the reader to [22]. The parameter s_k is known as the *stencil*. Neural networks following this construction are called *convolutional* (CNN).

In practice, a CNN computes a linear combination of many convolutions at each time step, namely

$$F_k^{(j)}(z_k) = \sigma\left(\sum_{m=1}^{M_k} W(s_k^{(j,m)})z_k^{(m)} + b_k^{(j)}\right)$$

for $j = 1, 2, \ldots, M_{k+1}$ where $z_k = [z_k^{(1)}, \ldots, z_k^{(M_k)}]$ with each entry known as a *channel* and $M_k = 1$ if no convolutions were computed at the previous iteration. Finally we define $F_k(z_k) = [F_k^{(1)}(z_k), \ldots, F_k^{(M_{k+1})}(z_k)]$. The number of channels at each time step, the integer M_{k+1}, is a design choice which, along with the choice for the size of the stencils $s_k^{(j,m)}$, the dimension of the input, and the design of W determine the dimension of the image space d_{k+1} for the map F_k.

When employing convolutions, it is standard practice to sometimes place maps which compute certain statistics from the convolution. These operations are commonly referred to as *pooling*. They are dimension reducing and are usually thought of as a way of extracting the most important information from a convolution. We refer the reader to [24, 25, 28, 52, 76] for further details.

Designs of feed-forward neural networks usually employ both convolutional (with and without pooling) and dense layers. While the success of convolutional networks has mostly come from image classification or object detection tasks [41], they can be useful for any data with spatial correlations [8, 22]. To connect the complex notation presented in this section with the standard in machine learning literature, we will give an example of a deep convolutional neural network. We consider the task of classifying images of hand-written digits given in the MNIST dataset [45]. These are 28×28 grayscale images of which there are $N = 60\,000$ and

10 overall classes $\{0, \dots, 9\}$ hence we consider $\mathcal{X} = \mathbb{R}^{28\times 28} \cong \mathbb{R}^{784}$ and $\mathcal{Y}$ the space of probability vectors over $\mathbb{R}^{10}$. Figure 1 show a typical construction of a deep convolutional neural network for this task. The word deep is generally reserved for models with $n > 3$. Once the model has been fit, figure 2 shows the output of each map on an example image. Starting with the digitized digit 0, the model computes its important features, through a sequence of operations involving convolutional layers, culminating in the second to last plot, the output of the affine map A. This plot shows model determining that the most likely digit is 0, but also giving substantial probability weight on the digit 6. This makes sense, as the digits 0 and 6 can look quite similar, especially when hand-written. Once the softmax is taken (because it exponentiates), the probability of the image being a 6 is essentially washed out, as shown in the last plot. This is a short-coming of the softmax as it may not accurately retain the confidence of the model's prediction. We stipulate that this may be a reason for the emergence of highly-confident adversarial examples [23, 74], but do not pursue suitable modifications in this work.

4. Algorithms

Section 4.1 describes the choice of loss function. Section 4.2 outlines the state-of-the-art derivative based optimization, with section 4.2.1 presenting the algorithms and section 4.2.2 presenting tricks for better convergence. Section 4.3 defines the EKI method, with subsequent subsections presenting our various modifications.

4.1. Loss function

Before delving into the specifics of optimization methods used, we discuss the general choice of loss function $\mathcal{L}$. While the machine learning literature contains a wide variety of loss functions that are designed for specific problems, there are two which are most commonly used and considered first when tackling any regression and classification problems respectively, and on which we focus our work in this paper. For regression tasks, the squared-error loss

$$\mathcal{L}(y', y) = \|y - y'\|_{\mathcal{Y}}^2$$

is standard and is well known to the inverse problems community; it arises from an additive Gaussian noise model. When the task at hand is classification, the standard choice of loss is the cross-entropy

$$\mathcal{L}(y', y) = -\langle y, \log y' \rangle_{\mathcal{Y}},$$

with the log computed point-wise and where we consider $\mathcal{Y} = \mathbb{R}^m$. This loss is well-defined on the space $\mathbb{P}_0^m \times \mathbb{P}^m$. It is consistent with the the projection map S of the neural network model being the softmax as $\mathrm{Im}(S) = \mathbb{P}_0^m$. A simple Lagrange multiplier argument shows that $\mathcal{L}$ is indeed infimized over $\mathbb{P}_0^m$ by sequence $y' \to y$ and hence the loss is consistent with what we want our model output to be[1]. From a modeling perspective, the choice of softmax as the output layer has some drawbacks as it only allows us to asymptotically match the data. However it is a good choice if the cross-entropy loss is used to solve the problem; indeed, in practice, the softmax along with the cross-entropy loss has seen the best numerical results when compared to other choices of thresholding/loss pairs [22].

[1] Note that the infimum is not, in general, attained in $\mathbb{P}_0^m$ as defined, because perfectly labeled data may take the form $\{y \in \mathbb{R}^m \mid \exists! j \text{ s.t. } y_j = 1, y_k = 0\ \forall k \neq j\}$ which is in the closure of $\mathbb{P}_0^m$ but not in $\mathbb{P}_0^m$ itself.

Convolutional Neural Network		
Map	**Type**	**Notation**
$F_0 : \mathbb{R}^{28\times 28} \to \mathbb{R}^{32\times 24\times 24}$	Conv 32x5x5	$M_0 = 1, M_1 = 32, s_0^{(j,m)} \in \mathbb{R}^{5\times 5}$ $j \in \{1,\dots,32\}, m = \{1\}$
$F_1 : \mathbb{R}^{32\times 24\times 24} \to \mathbb{R}^{32\times 10\times 10}$	Conv 32x5x5 MaxPool 2x2	$M_2 = 32, s_1^{(j,m)} \in \mathbb{R}^{5\times 5}$ $j \in \{1,\dots,32\}, m \in \{1,\dots,32\}$ $H_1 = H_2 = 2$ $(\alpha = \beta = 2)$
$F_2 :: \mathbb{R}^{32\times 10\times 10} \to \mathbb{R}^{64\times 6\times 6}$	Conv 64x5x5	$M_3 = 64, s_2^{(j,m)} \in \mathbb{R}^{5\times 5}$ $j \in \{1,\dots,64\}, m \in \{1,\dots,32\}$
$F_3 : \mathbb{R}^{64\times 6\times 6} \to \mathbb{R}^{64}$	Conv 64x5x5 MaxPool 2x2 (global)	$M_4 = 64, s_3^{(j,m)} \in \mathbb{R}^{5\times 5}$ $j \in \{1,\dots,64\}, m \in \{1,\dots,64\}$ $H_1 = H_2 = 2$
$F_4 : \mathbb{R}^{64} \to \mathbb{R}^{500}$	FC-500	$W_4 \in \mathbb{R}^{500\times 64}, b_4 \in \mathbb{R}^{500}$
$A : \mathbb{R}^{500} \to \mathbb{R}^{10}$	FC-10	$W_5 \in \mathbb{R}^{10\times 500}, b_5 \in \mathbb{R}^{10}$
$S : \mathbb{R}^{10} \to \mathbb{R}^{10}$	Softmax	$S(w) = \frac{1}{\sum_{j=1}^{10} e^{w_j}}(e^{w_1},\dots,e^{w_{10}})$

Figure 1. A four layer convolutional neural network for classifying images in the MNIST data set. The middle column shows a description typical of the machine learning literature. The other two columns connect this jargon to the notation presented here. No padding is added and the convolutions are computed over maximally overlapping blocks (stride of one). The nonlinearity σ is the ReLU and is the same for every layer.

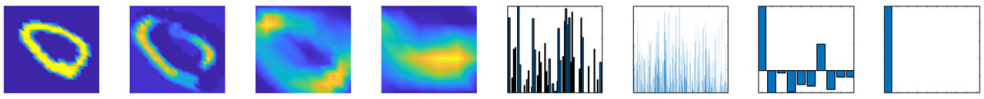

Figure 2. Output of each map from left to right of the convolutional neural network shown in figure 1. The left most image is the input and the next three images show a single randomly selected channel from the outputs of F_0, F_1, F_2 respectively. The outputs of F_3, F_4, A, S are vectors shown respectively in the four subsequent plots. We see that with high probability the network determines that the image belongs to the first class (0) which is correct.

The interpretation of the cross-entropy loss is to think of our model as approximating a categorical distribution over the input data and, to get this approximation, we want to minimize its Shannon cross-entropy with respect to the data. Note, however, that there is no additive noise model for which this loss appears in the associated MAP estimator simply because $\mathcal{L}$ cannot be written purely as a function of the residual $y - y'$.

4.2. Gradient based optimization

4.2.1. The iterative technique. The current state of the art for solving optimization problems of the form (2), (4) and (6) is based around the use of stochastic gradient descent (SGD) [37, 61, 65]. We will describe these methods starting from a continuous time viewpoint, for pedagogical clarity. In particular, we think of the unknown parameter as the large time limit of a smooth function of time $u : [0,\infty) \to \mathcal{U}$. Let $\Phi(u;\mathsf{x},\mathsf{y}) = \Phi_{\mathrm{s}}(u;\mathsf{x},\mathsf{y})$ or $\Phi_{\mathrm{ss}}(u;\mathsf{x},\mathsf{y})$ then gradient descent imposes the dynamic

$$\dot{u} = -\nabla\Phi(u;\mathsf{x},\mathsf{y}), \quad u(0) = u_0 \tag{10}$$

which moves the parameter in the steepest descent direction with respect to the regularized loss function, and hence will converge to a local minimum for Lebesgue almost all initial data, leading to bounded trajectories [46, 69].

For the practical implementations of this approach in machine learning, a number of adaptations are made. First the ODE is discretized in time, typically by a forward Euler scheme; the time-step is referred to as the *learning rate*. The time-step is often, but not always, chosen to be a decreasing function of the iteration step [15, 61]. Secondly, at each step of the iteration, only a subset of the data is used to approximate the full gradient. In the supervised case, for example,

$$\Phi_{\mathrm{s}}(u;\mathsf{x},\mathsf{y}) \approx \frac{1}{N'}\sum_{j\in B_{N'}} \mathcal{L}(\mathcal{G}(u|x_j), y_j) + R(u)$$

where $B_{N'} \subset \{1,\dots,N\}$ is a random subset of cardinality N' usually with $N' \ll N$. A new $B_{N'}$ is drawn at each step of the Euler scheme without replacement until the full dataset has been exhausted. One such cycle through all of the data is called an *epoch*. The number of epochs it takes to train a model varies significantly based on the model and data at hand but is usually within the range 10–500. This idea, called *mini-batching*, leads to the terminology *stochastic gradient descent (SGD)*. Recent work has suggested that adding this type of noise helps preferentially guide the gradient descent towards places in parameter space which generalize better than standard descent methods [12, 13].

A third variant on basic gradient descent is the use of momentum-augmented methods utilized to accelerate convergence [54]. The deep theory associated with these methods relates to a clever adaptive choice of momentum which changes with the step of the algorithm; however as used in machine lerning practice the momentum level is typically fixed. Various continuous time dynamics associated with the Nesterov momentum method can be found in [40, 70] and take the form

$$\begin{aligned} &m\ddot{u} + \gamma(t)\dot{u} = -\nabla\Phi(u;\mathsf{x},\mathsf{y}),\\ &u(0) = u_0, \quad \dot{u}(0) = 0. \end{aligned} \tag{11}$$

From these variants on continuous time gradient descent have come a plethora of adaptive first-order optimization methods that attempt to solve the learning problem. Some of the more popular include Adam, RMSProp, and Adagrad [16, 38]. There is no consensus on which methods performs best although some recent work has argued in favor of SGD and momentum SGD [81].

Lastly, the online learning problem (6) is also commonly solved via a gradient descent method dubbed online gradient descent (OGD). The dynamic is

$$\begin{aligned} &\dot{u}_j = -\nabla\Phi_{\mathrm{o}}(u_j, u_{j-1}; x_j, y_j)\\ &u_j(0) = u_{j-1}(T) \end{aligned}$$

which can be extended to the momentum case in the obvious way. It is common that only a single step of the Euler scheme is computed. The process of letting all these ODE(s) evolve in time is called *training*.

4.2.2. Initialization. A major challenge for the iterative methods presented here is finding a good starting point u_0 for the dynamic; a problem usually termed *initialization* .Historically, initialization was first dealt with using a technique called *layer-wise pretraining* [29]. In this approach the parameters are initialized randomly. Then the parameters of all but first layer are held fixed and SGD is used to find the parameters of the first layer. Then all but the

parameters of the second layer are held fixed and SGD is used to find the parameters of the second layer. Repeating this for all layers yields an estimate u_0 for all the parameters, and this is then used as an initialization for SGD in a final step called *fine-tuning*. Development of new activation functions, namely the ReLU, has allowed simple random initialization (from a carefully designed prior measure) to work just as well, making layer-wise pretraining essentially obsolete. There are many proposed strategies in the literature for how one should design this prior [21, 50]. The main idea behind all of them is to somehow normalize the output mean and variance of each map F_k. One constructs the product probability measure

$$\mu_0 = \mu_0^{(0)} \otimes \mu_0^{(1)} \otimes \cdots \otimes \mu_0^{(n-1)} \otimes \mu_0^{(n)}$$

where each $\mu_0^{(k)}$ is usually a centered, isotropic probability measure with covariance scaling γ_k. Each such measure corresponds to the distribution of the parameters of each respective layer with $\mu_0^{(n)}$ attached to the parameters of the map A. A common strategy called Xavier initialization [21] proposes that the inverse covariance (precision) is determined by the average of the input and output dimensions of each layer:

$$\gamma_k^{-1} = \frac{1}{2}(d_k + d_{k+1})$$

thus

$$\gamma_k = \frac{2}{d_k + d_{k+1}}.$$

When the layer is convolutional, d_k and d_{k+1} are instead taken to be the number of input and output channels times the size of each stencil respectively. Usually each $\mu_0^{(k)}$ is then taken to be a centered Gaussian or uniform probability measure. Once this prior is constructed one initializes SGD by a single draw.

4.3. Ensemble Kalman inversion

The ensemble Kalman filter (EnKF) is a method for estimating the state of a stochastic dynamical system from noisy observations [18]. Over the last decade the method has been systematically developed as an iterative method for solving general inverse problems; in this context, it is sometimes referred to as ensemble Kalman inversion (EKI) [34]. Viewed as a sequential Monte Carlo method [67], it works on an ensemble of parameter estimates (particles) transforming them from the prior into the posterior. Recent work has established, however, that unless the forward operator is linear and the additive noise is Gaussian [67], the correct posterior is not obtained [19]. Nevertheless there is ample numerical evidence that shows EKI works very well as a derivative-free optimization method for nonlinear least-squares problems [5, 36]. In this paper, we view it purely through the lens of optimization and propose several modifications to the method that follow from adopting this perspective within the context of machine learning problems.

Consider the general inverse problem

$$\mathsf{y} = \mathsf{G}(u) + \eta$$

where $\eta \sim \pi = N(0, \Gamma)$ represent noise, and let μ_0 be a prior measure on the parameter u. Note that the supervised, semi-supervised, and online learning problems (8) and (9) can be put into this general framework by adjusting the number of data points in the concatenations y, x

and letting x be absorbed into the definition of G. Let $\{u^{(j)}\}_{j=1}^J \subset \mathcal{U}$ be an ensemble of parameter estimates which we will allow to evolve in time through interaction with one another and with the data; this ensemble may be initialized by drawing independent samples from μ_0, for example. The evolution of $u^{(j)} : [0, \infty) \to \mathcal{U}$ is described by the EKI dynamic [67]

$$\begin{aligned} \dot{u}^{(j)} &= -C^{\mathrm{uw}}(u)\Gamma^{-1}(\mathsf{G}(u^{(j)}) - \mathsf{y}), \\ u^{(j)}(0) &= u_0^{(j)}. \end{aligned}$$

Here

$$\bar{\mathsf{G}} = \frac{1}{J}\sum_{l=1}^{J} \mathsf{G}(u^{(l)}), \quad \bar{u} = \frac{1}{J}\sum_{l=1}^{J} u^{(l)}$$

and $C^{\mathrm{uw}}(u)$ is the empirical cross-covariance operator

$$C^{\mathrm{uw}}(u) = \frac{1}{J}\sum_{j=1}^{J}(u^{(j)} - \bar{u}) \otimes (\mathsf{G}(u^{(j)}) - \bar{\mathsf{G}}).$$

Thus

$$\begin{aligned} \dot{u}^{(j)} &= -\frac{1}{J}\sum_{k=1}^{J}\langle \mathsf{G}(u^{(k)}) - \bar{\mathsf{G}}, \mathsf{G}(u^{(j)}) - \mathsf{y}\rangle_\Gamma \, u^{(k)}, \\ u^{(j)}(0) &= u_0^{(j)}. \end{aligned} \tag{12}$$

Viewing the difference of $\mathsf{G}(u^{(k)})$ from its mean, appearing in the left entry of the inner-product, as a projected approximate derivative of G, it is possible to understand (12) as an approximate gradient descent.

Rigorous analysis of the long-term properties of this dynamic for a finite J are poorly understood except in the case where $\mathsf{G}(\cdot) = A\cdot$ is linear [67]. In the linear case, we obtain that $u^{(j)} \to u^*$ as $t \to \infty$ where u^* minimizes the functional

$$\Phi(u; \mathsf{y}) = \frac{1}{2}\|\mathsf{y} - Au\|_\Gamma^2$$

in the subspace $\mathcal{A} = \mathrm{span}\{u_0^{(j)} - \bar{u}\}_{j=1}^J$, and where $\bar{u}$ is the mean of the initial ensemble $\{u_0^{(j)}\}$. This follows from the fact that, in the linear case, we may re-write (12) as

$$\dot{u}^{(j)} = -C(u)\nabla_u \Phi(u^{(j)}; \mathsf{y})$$

where $C(u)$ is an empirical covariance operator

$$C(u) = \frac{1}{J}\sum_{j=1}^{J}(u^{(j)} - \bar{u}) \otimes (u^{(j)} - \bar{u}).$$

Hence each particle performs a gradient descent with respect to Φ and $C(u)$ projects into the subspace $\mathcal{A}$.

To understand the nonlinear setting we use linearization. Note from (12) that

$$\begin{aligned}\dot{u}^{(j)} &= -\frac{1}{J}\sum_{k=1}^{J}\langle \mathsf{G}(u^{(k)}) - \frac{1}{J}\sum_{l=1}^{J}\mathsf{G}(u^{(l)}), \mathsf{G}(u^{(j)}) - \mathsf{y}\rangle_\Gamma \, u^{(k)} \\ &= -\frac{1}{J}\sum_{k=1}^{J}\langle \mathsf{G}(u^{(k)}) - \frac{1}{J}\sum_{l=1}^{J}\mathsf{G}(u^{(l)}), \mathsf{G}(u^{(j)}) - \mathsf{y}\rangle_\Gamma \, (u^{(k)} - \bar{u}) \\ &= -\frac{1}{J^2}\sum_{k=1}^{J}\sum_{l=1}^{J}\langle \mathsf{G}(u^{(k)}) - \mathsf{G}(u^{(l)}), \mathsf{G}(u^{(j)}) - \mathsf{y}\rangle_\Gamma \, (u^{(k)} - \bar{u}).\end{aligned}$$

Now we linearize on the assumption that the particles are close to one another, so that

$$\begin{aligned}\mathsf{G}(u^{(k)}) &= \mathsf{G}(u^{(j)} + u^{(k)} - u^{(j)}) \approx \mathsf{G}(u^{(j)}) + D\mathsf{G}(u^{(j)})(u^{(k)} - u^{(j)}) \\ \mathsf{G}(u^{(l)}) &= \mathsf{G}(u^{(j)} + u^{(l)} - u^{(j)}) \approx \mathsf{G}(u^{(j)}) + D\mathsf{G}(u^{(j)})(u^{(l)} - u^{(j)}).\end{aligned}$$

Here $D\mathsf{G}$ is the Fréchet derivative of G. With this approximation, we obtain

$$\begin{aligned}\dot{u}^{(j)} &\approx -\frac{1}{J^2}\sum_{k=1}^{J}\sum_{l=1}^{J}\langle D\mathsf{G}^*(u^{(j)})(\mathsf{G}(u^{(j)}) - \mathsf{y}), u^{(k)} - u^{(l)}\rangle_\Gamma (u^{(k)} - \bar{u}) \\ &= -\frac{1}{J}\sum_{k=1}^{J}\langle D\mathsf{G}^*(u^{(j)})(\mathsf{G}(u^{(j)}) - \mathsf{y}), u^{(k)} - \bar{u}\rangle_\Gamma (u^{(k)} - \bar{u}) \\ &= -C(u)\nabla_u \Phi(u^{(j)}, \mathsf{y})\end{aligned}$$

where

$$\Phi(u; \mathsf{y}) = \frac{1}{2}\|\mathsf{y} - \mathsf{G}(u)\|_\Gamma^2.$$

This is again just gradient descent with a projection onto the subspace $\mathcal{A}$. These arguments also motivate the interesting variants on EKI proposed in [26]; indeed the paper [26] inspired the organization of the linearization calculations above.

In summary, the EKI is a methodology which behaves like gradient descent, but achieves this without computing gradients. Instead it uses an ensemble and is hence inherently parallelizable. In the context of machine learning this opens up the possibility of avoiding explicit backpropagation, and doing so in a manner which is well-adapted to emerging computer architectures.

4.3.1. Cross-entropy loss. The previous considerations demonstrate that EKI as typically used is closely related to minimizing an ℓ_2 loss function via gradient descent. Here we propose a simple modification to the method allowing it to minimize any loss function instead of only the squared-error; our primary motivation is the case of cross-entropy loss.

Let $\mathcal{L}(\mathsf{y}', \mathsf{y})$ be any loss function, this may, for example, be the cross entropy

$$\mathcal{L}(\mathsf{y}', \mathsf{y}) = -\frac{1}{N}\langle \mathsf{y}, \log \mathsf{y}'\rangle_{\mathcal{Y}^N}.$$

Now consider the dynamic

$$\begin{aligned}\dot{u}^{(j)} &= -C^{\mathrm{uw}}(u)\nabla_{\mathsf{y}'}\mathcal{L}(\mathsf{G}(u^{(j)}), \mathsf{y}) \\ &= -\frac{1}{J}\sum_{k=1}^{J}\langle \mathsf{G}(u^{(k)}) - \bar{\mathsf{G}}, \nabla_{\mathsf{y}'}\mathcal{L}(\mathsf{G}(u^{(j)}), \mathsf{y})\rangle \, u^{(k)}.\end{aligned} \tag{13}$$

If $\mathcal{L}(\mathsf{y}', \mathsf{y}) = \frac{1}{2}\|\mathsf{y} - \mathsf{y}'\|_\Gamma^2$ then $\nabla_{\mathsf{y}'}\mathcal{L}(\mathsf{G}(u^{(j)}), \mathsf{y}) = \Gamma^{-1}(\mathsf{G}(u^{(j)}) - \mathsf{y})$ recovering the original dynamic. Note that since we've defined the loss through the auxiliary variable y' which is meant to stand-in for the output of our model, the method remains derivative-free with respect to the model parameter u, but does not allow for adding regularization directly into the loss. However regularization could be added directly into the dynamic; we leave such considerations for future work.

An interpretation of the original method is that it aims to make the norm of the residual $\mathsf{y} - \mathsf{G}(u^{(j)})$ small. Our modified version replaces this residual with $\nabla_{\mathsf{y}'}\mathcal{L}(\mathsf{G}(u^{(j)}), \mathsf{y})$, but when $\mathcal{L}$ is the cross entropy this is in fact the same (in the ℓ_1 sense). We make this precise in the following proposition.

Proposition 1. *Let $\mathsf{G} : \mathcal{U} \to (\mathbb{P}_0^m)^N$ and suppose $\mathsf{y} = [e_{k_1}, \dots, e_{k_N}]^T$ where e_{k_j} is the k_jth standard basis vector of $\mathbb{R}^m$. Then $u^* \in \mathcal{U}$ is a solution to*

$$\arg\min_{u\in\mathcal{U}} \|\mathsf{y} - \mathsf{G}(u)\|_{\ell_1}$$

if and only if u^* is a solution to

$$\arg\min_{u\in\mathcal{U}} \|\nabla_{\mathsf{y}'}\mathcal{L}(\mathsf{G}(u), \mathsf{y})\|_{\ell_1}$$

where $\mathcal{L}(\mathsf{y}', \mathsf{y}) = -\langle \mathsf{y}, \log \mathsf{y}'\rangle_{\ell_2}$ is the cross-entropy loss.

Proof. Without loss of generality, we may assume $N = 1$ and thus let $\mathsf{y} = e_k$ be the kth standard basis vector of $\mathbb{R}^m$. Suppose that u^* is a solution to $\arg\min_{u\in\mathcal{U}} \|\mathsf{y} - \mathsf{G}(u)\|_{\ell_1}$. Then for any $u \in \mathcal{U}$, we have

$$\sum_{j\neq k} \mathsf{G}(u^*)_j + (1 - \mathsf{G}(u^*)_k) \leqslant \sum_{j\neq k} \mathsf{G}(u)_j + (1 - \mathsf{G}(u)_k).$$

Adding $0 = \mathsf{G}(u^*)_k - \mathsf{G}(u^*)_k$ to the l.h.s. and $0 = \mathsf{G}(u)_k - \mathsf{G}(u)_k$ to the r.h.s. and noting that $\|\mathsf{G}(u)\|_{\ell_1} = 1$ for all $u \in \mathcal{U}$ since $\mathrm{Im}(\mathsf{G}) = \mathbb{P}_0^m$ we obtain

$$2(1 - \mathsf{G}(u^*)_k) \leqslant 2(1 - \mathsf{G}(u)_k)$$

which implies

$$\frac{1}{\mathsf{G}(u^*)_k} \leqslant \frac{1}{\mathsf{G}(u)_k}$$

as required since $\|\nabla_{\mathsf{y}'}\mathcal{L}(\mathsf{G}(u), \mathsf{y})\|_{\ell_1} = 1/\mathsf{G}(u)_k$. The other direction follows similarly. □

4.3.2. Momentum. Continuing in the spirit of optimization, we may also add Nesterov momentum to the EKI method. This is a simple modification to the dynamic (13),

$$\begin{aligned} &\ddot{u}^{(j)} + \frac{3}{t}\dot{u}^{(j)} = -C^{\mathrm{uw}}(u)\nabla_{\mathsf{y}'}\mathcal{L}(\mathsf{G}(u^{(j)}); \mathsf{y}) \\ &u^{(j)}(0) = u_0^{(j)}, \quad \dot{u}^{(j)}(0) = 0. \end{aligned} \tag{14}$$

While we present momentum EKI in this form, in practice, we follow the standard in machine learning by fixing a momentum factor $\lambda \in (0, 1)$ and discretizing (13) using the method shown in section 4.2.1. In standard stochastic gradient decent, it has been observed that this

discretization converges more quickly and possibly to a better local minima than the forward Euler discretization [72]. Numerically, we discover a similar speed up for EKI. However, the memory cost doubles as we need to keep track of an ensemble of positions and momenta. Some experiments in the next section demonstrate the speed-up effect. We leave analysis and possible applications to other inverse problems of the momentum method as presented in (14) for future work.

4.3.3. Discrete scheme. Finally we present our modified EKI method in the implementable, discrete time setting and discuss some variants on this basic scheme which are particularly useful for machine learning problems. In implementation, it is useful to consider the concatenation of particles $\mathsf{u} = [u^{(1)}, \dots, u^{(J)}]$ which may be viewed as a function $\mathsf{u} : [0, \infty) \to \mathcal{U}^J$. Then (13) becomes

$$\dot{\mathsf{u}} = -D(\mathsf{u})\mathsf{u}$$

where for each fixed u the operator $D(\mathsf{u}) : \mathcal{U}^J \to \mathcal{U}^J$ is a linear operator. Suppose $\mathcal{U} = \mathbb{R}^P$ then we may exploit symmetry and represent $D(\mathsf{u})$ by a $J \times J$ matrix instead of a $JP \times JP$ matrix. To this end, suppose the ensemble members are stacked row-wise that is $\mathsf{u} \in \mathbb{R}^{J \times P}$ then $D(\mathsf{u})$ has the simple representation

$$(D(\mathsf{u}))_{kj} = \langle \mathsf{G}(u^{(k)}) - \bar{\mathsf{G}}, \nabla_{y'} \mathcal{L}(\mathsf{G}(u^{(j)}), \mathsf{y}) \rangle$$

which is readily verified by (13). We then discretize via an adaptive forward Euler scheme to obtain

$$\mathsf{u}_{k+1} = \mathsf{u}_k - h_k D(\mathsf{u}_k)\mathsf{u}_k.$$

Choosing the correct time-step has an immense impact on practical performance. We have found that the choice

$$h_k = \frac{h_0}{\|D(\mathsf{u}_k)\|_F + \epsilon},$$

where $\|\cdot\|_F$ denotes the Frobenius norm, works well in practice [17]. We aim to make h_0 as large as possible without loosing stability of the dynamic. The intuition behind this choice has to do with the fact that that $D(\mathsf{u})$ measures how close the propagated particles are to each other (left part of the inner-product) and how close they are to the data (right part of the inner-product). When either or both of these are small, we may take larger steps, and still retain numerical stability, by choosing h_k inversely proportional to $\|D(\mathsf{u})\|_F$; the parameter ϵ is added to avoid floating point issues when $\|D(\mathsf{u})\|_F$ is near machine precision. As $k \to \infty$, we typically match the data with increasing accuracy and, simultaneously, the propagated particles achieve consensus and collapse on one another; as a consequence $\|D(\mathsf{u}_k)\|_F \to 0$ which means we take larger and larger steps. Note that this is in contrast to the Robbins–Monro implementation of stochastic gradient descent where the sequence of time-steps are chosen to decay monotonically to zero.

Similarly, the momentum discretization of (13) is

$$\begin{aligned}\mathsf{u}_{k+1} &= \mathsf{v}_k - h_k D(\mathsf{v}_k)\mathsf{v}_k \\ \mathsf{v}_{k+1} &= \mathsf{u}_{k+1} + \lambda(\mathsf{u}_{k+1} - \mathsf{u}_k)\end{aligned}$$

with $\lambda \in (0, 1)$ fixed, $\mathsf{u}_0 = \mathsf{v}_0$ where $h_k = h_0/(\|D(\mathsf{v}_k)\|_F + \epsilon)$ as before and v represent the particle momenta.

We now present a list of numerically successful heuristics that we employ when solving practical problems.

(I) Initialization To construct the initial ensemble, we draw an i.i.d. sequence $\{u_0^{(j)}\}_{j=1}^J$ with $u_0^{(1)} \sim \mu_0$ where μ_0 is selected according to the construction discussed for initialization of the neural network model in the section outlining SGD.

(II) Mini-batching We borrow from SGD the idea of mini-batching where we use only a subset of the data to compute each step of the discretized scheme, picking randomly without replacement. As in the classical SGD context, we call a cycle through the full dataset an epoch.

(III) Prediction In principle, any one of the particles $u^{(j)}$ can be used as the parameters of the trained model. However, as analysis of figure 7 below shows, the spread in their performance is quite small; furthermore even though the system is nonlinear, the mean particle $\bar{u}$ achieves an equally good performance as the individual particles. Thus, for computational simplicity, we choose to use the mean particle as our final parameter estimate. This choice further motivates one of the ways in which we randomize.

(V) Randomization The EKI property that all particles remain in the subspace spanned by the initial ensemble is not desirable when $J \ll \dim \mathcal{U}$. We break this property by introducing noise into the system. We have found two numerically successful ways of accomplishing this.

i. At each step of the discrete scheme, add noise to each particle,

$$u_k^{(j)} \mapsto u_k^{(j)} + \eta_k^{(j)}$$

where $\{\eta_k^{(j)}\}_{j=1}^J$ is an i.i.d. sequence with $\eta_k^{(1)} \sim \mu_k$. We define μ_k to be a scaled version of μ_0 by scaling its covariance operator namely $C_k = \sqrt{h_k} C_0$, where h_k is the time step as previously defined. Note that as the particles start to collapse, h_k increases, hence we add more noise to counteract this. In the momentum case, we perform the same mapping but on the particle momenta instead

$$v_k^{(j)} \mapsto v_k^{(j)} + \eta_k^{(j)}.$$

ii. At the end of each epoch, randomize the particles around their mean,

$$u_{kT}^{(j)} \mapsto \bar{u}_{kT} + \eta_{kT}^{(j)}$$

where T is the number of steps needed to complete a cycle through the entire dataset and $\{\eta_{kT}^{(j)}\}_{j=1}^J$ is an i.i.d. sequence with $\eta_{kT}^{(1)} \sim \mu_0$. Note that because this randomization is only done after a full epoch, it is not clear how the noise should be scaled and thus we simply use the prior. This may not be the optimal thing to do, but we have found great numerical success with this strategy. Figure 8 shows the spread of the ratio of the parameters to the the noise $\|\bar{u}_{kT}\|/\|\eta_{kT}^{(j)}\|$. We see that relatively less noise is added as training continues. It may be possible to achieve better results by increasing the noise with time as to combat collapse. However, we do not perform such experiments. Furthermore we have found that this does not work well in the momentum case; hence all randomization for the momentum scheme is done according to the first point.

(V) Expanding ensemble Numerical experiments show that using a small number of particles tends to have very good initial performance (one to two epochs) that quickly saturates. On the other hand, using a large number of particles does not do well to begin with but greatly outperforms small particle ensembles in the long run. Thus we use the idea of an expanding ensemble where we gradually add in new particles. This is done in the context of point (ii.) of the randomization section. Namely, at the end of an epoch, we compute the ensemble mean and create a new larger ensemble by randomizing around it.

Lastly we mention that, in many inverse problem applications, it is good practice to randomize the data for each particle at each step [42] namely map

$$\mathsf{y} \mapsto \mathsf{y} + \xi_k^{(j)}$$

where $\{\xi_k^{(j)}\}_{j=1}^J$ is an i.i.d. sequence with $\xi_k^{(1)} \sim \pi$. However we have found that this does not work well for classification problems. This may be because the given classifications are correct and there is no actual noise in the data. Such noise may thus be biased in the classification setting. We have not experimented in the case where the labels are noisy and leave this for future work.

5. Numerical experiments

In the following set of experiments, we demonstrate the wide applicability of EKI on several machine learning tasks. All forward models we consider are some type of neural network, except for the semi-supervised learning case where we consider the construction in example 2.2. While, for the sake of brevity, we do not give details on recurrent neural networks in this work, we refer the reader to [22] for details. We benchmark EKI against SGD and momentum SGD and do not consider any other first-order adaptive methods. Recent work has shown that their value is only marginal and the solutions they find may not generalize as well [81]. Furthermore we do not employ batch normalization as it is not clear how it should be incorporated with EKI methods. However, when batch normalization is necessary, we instead use the SELU nonlinearity [39], finding the performance to be essentially identical to batch normalization on problems where we have been able to compare.

The next five subsections are organized as follows. Section 5.1 contains the conclusions drawn from the experiments. In section 5.2, we describe the six data sets used in all of our experiments as well as the metrics used to evaluate the methods. Section 5.3 gives implementation details and assigns methods using different techniques their own name. In sections 5.4–5.6 we show the supervised, semi-supervised, and online learning experiments respectively. Since most of our experiments are supervised, we split section 5.4 based on the type of model used namely dense neural networks, convolutional neural networks, and recurrent neural networks respectively.

5.1. Summary of numerical results

The following are the primary conclusion of our numerical experiments:

- On supervised classification problems with a feed-forward neural network, EKI performs just as well as SGD even when the number of unknown parameters is up to two order of magnitude larger than the ensemble size. Furthermore EKI seems more numerically stable than SGD, as seen in the smaller amount of oscillation in the test accuracy, and requires less hyper-parameter tuning. In fact, the only parameter we vary in our experiments is the number of ensemble members, and we do this simply to demonstrate its

effect. However due to the large number of forward passes required at each EKI iteration, we have found the method to be significantly slower than SGD. Due to the very efficient implementations of backpropagation a single backward-pass is comparable in wall-clock time to single forward-pass, and EKI requires J forward-passes at each iteration. This issue can be mitigated if each of the forward computations is parallelized across multiple processing units, as it often is in many industrial applications [32, 56, 57]. We leave such computational considerations for future work, as our current goal is simply to establish proof of concept. Our experiments are conducted on neural networks of up to half a million parameters which is very small compared to modern deep learning architectures. We choose such small networks to allow for rapid parallel prototyping, but note that the algorithms are inherently parallelizable and should scale well. Furthermore, as our CNN experiments point out, EKI can handle relatively deep, narrow architectures which are considered difficult to train in the machine learning literature [50, 62]. In addition, recent work such as [1] suggests that huge over-parameterization makes the associated optimization problem easier, indicating promise for EKI when used for networks with tens of millions of parameters. These experiments can be found in the first two subsections of section 5.4.

- On supervised classification problems with a recurrent neural network, EKI significantly outperforms SGD on the small problems we consider. This is likely due to the steep barriers that occur on the loss surface of recurrent networks [4, 58] which EKI may be able to avoid due to its noisy Jacobian estimates. These experiments can be found in the last subsection of section 5.4.
- On the semi-supervised learning problem we consider, EKI does not perform as well as state of the art (MCMC) [7], but performs better than the naive solution. However, even with a large number of ensemble members, EKI is much faster and computationally cheaper than MCMC, allowing applications to large scale problems. These experiments can be found in section 5.5.
- On online regression problems tackled with a recurrent neural network, EKI converges significantly faster and to a better solution than SGD with $\mathcal{O}(1)$ ensemble members. While the problems we consider are only simple, univariate time-series, the results demonstrate great promise for harder problems. It has long been known that recurrent neural networks are very hard to optimize with gradient-based techniques [58], so we are very hopeful that EKI can improve on current state of the art. Again, we leave such domain specific applications to future work. These experiments can be found in section 5.6.

5.2. Data sets

We consider four data sets where the problem at hand is classification and two data sets where it is regression. For classification, three of the data sets are comprised of images and the third of voting histories. Our goal is to classify the image based on its content or classify the voting record based on party affiliation. For regression, both datasets are univariate time-series and our goal is to predict an unobserved part of the series. Figure 3 shows samples from each of the data sets.

As outlined in section 2, the goal of learning is to find a model which generalizes well to unobserved data. Thus, to evaluate this criterion, we split all data sets into a training and a testing portion. The training portion is used when we let our ODE(s) evolve in time as described in section 4. The testing portion is used only to evaluate the model. In other contexts, the training set is further split to create a validation set, but, since we perform no hyper-parameter

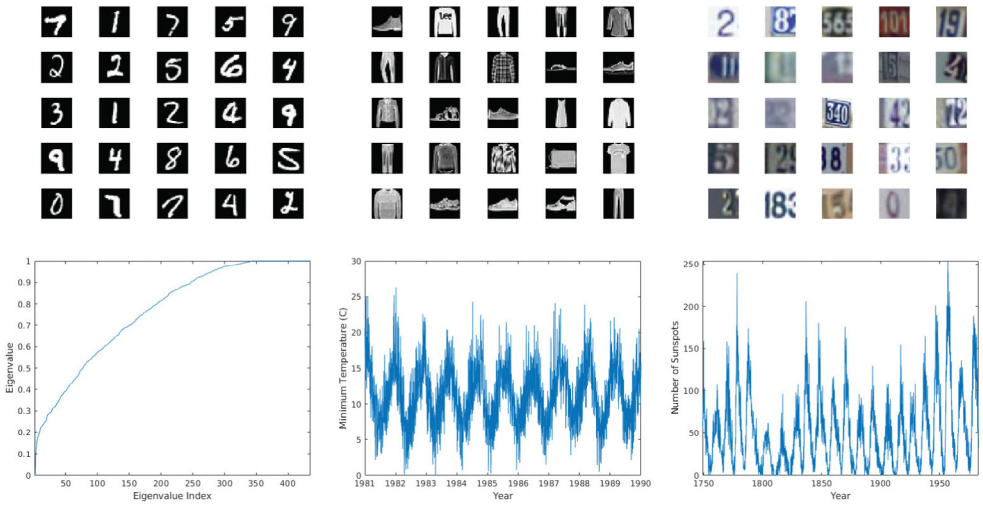

Figure 3. The six data sets used in numerical experiments. The first row shows 25 samples from MNIST, FashionMNIST, and SVHN respectively. The second row shows the spectrum of graph Lalpacian for the voting records data set, the full time-series for the daily minimum temperatures in Melbourne, and the monthly number of sunspots from Zürich respectively.

tuning, we omit this step. For classification, the metric we use is called *test accuracy*. This is the total number of correctly classified examples divided by the total number of examples in the test set. For regression, the metric we use is called *test error*. This is the average (across the test set) squared ℓ_2-norm of the difference between the true value and our prediction.

5.2.1. Classification. The first data set we consider is MNIST [45]. It contains 70 000 images of hand-written digits. All examples are 28×28 grayscale images and each is given a classification in $\{0, \dots, 9\}$ depending on what digit appears in the image. Thus we consider $\mathcal{X} = \mathbb{R}^{28\times 28} \cong \mathbb{R}^{784}$ and $\mathcal{Y} = \mathbb{P}^{10}$. Each of the labels y_j is a standard basis vector of $\mathbb{R}^{10}$ with the position of the one indicating the digit. We use 60 000 of the images for training and 10 000 for testing. Since grayscale values range from 0 to 255, all images are fist normalized to the range $[0, 1]$ by point-wise dividing by 255. Treating all training images as a sequence of $60\,000 \cdot 784$ numbers, their mean and standard deviation are computed. Each image (including the test set) is then again normalized via point-wise subtraction by the mean and point-wise division by the standard deviation. This data normalization technique is standard in machine learning.

The second image data set we consider is FashionMNIST [82]. It contains 70 000 images of different types of clothing items. All examples are 28×28 grayscale images and each is given a classification in $\{0, \dots, 9\}$ depending on the type of clothing item pictured. We treat it in the exact same way that we treat MNIST.

The third image data set we consider is SVHN [55]. It contains 99 289 natural images of cropped house numbers taken from Google street view. All examples are 32×32 RGB images and each is given a classification in $\{0, \dots, 9\}$ depending on what digit appears in the image. Thus we consider $\mathcal{X} = \mathbb{R}^{3\times 32\times 32} \cong \mathbb{R}^{3072}$ and $\mathcal{Y} = \mathbb{P}^{10}$ with the labels again being basis vectors of $\mathbb{R}^{10}$. We use 73 257 of the images for training and 26 032 for testing. All values are first normalized to be in the range $[0, 1]$. We then perform the same normalization as in MNIST, but this time per channel. That is, for all training images, we treat each color channel

as a sequence of $73\,257 \cdot 1024$ numbers, compute the mean and standard deviation then normalize each channel as before.

The last data set for classification we consider contains the voting record of the 435 U.S. House of Representatives members; see [6] and references therein. The votes were recorded in 1984 from the 98th United States Congress, 2nd session. Each record is tied to a particular representative and is a vector in $\mathcal{X} = \mathbb{R}^{16}$ with each entry being $+1$, -1, or 0 indicating a vote for, against, or abstain respectively. The labels live in $\mathcal{Y} = \mathbb{R}$ and are $+1$ or -1 indicating Democrat or Republican respectively. We use this data set only for semi-supervised learning and thus pick the amount of observed labels $|Z'| = 5$ with two Republicans and three Democrats. No normalization is performed. When computing the test accuracy, we do so over the entire data sets namely we do not remove the five observed records.

5.2.2. Regression. The first data set we consider for regression is a time series of the daily minimum temperatures (in Celsius) in Melbourne, Australia from January 1st 1981 to December 31th 1990 [20]. It contains 3650 total observations of which we use the first 3001 for training (up to March 22nd 1989) and the rest for testing. We consider $\mathcal{X} = \mathcal{Y} = \mathbb{R}$ by letting (in the training set) the data be the first 3000 observations and the labels be the 2nd to 3001st observations i.e. a one-step-ahead split. The same is done for the testing set. The minimum and maximum values $x_{\min}$, $x_{\max}$ over the training set are computed and all data is transformed via

$$x_j \mapsto \frac{x_j - x_{\min}}{x_{\max} - x_{\min}}.$$

This ensures the training set is in the range $[0, 1]$ and the testing set will also be close to that range.

The second data set for regression is a time series containing the number of observed sunspots from Zürich, Switzerland during each month from January 1749 to December 1983 [2]. It contains 2820 observations of which we use the first 2301 for training (up to September 1915) and the rest for testing. The data is treated in exactly the same way as the temperatures data set.

5.3. Implementation details

Having outlined many different strategies for performing EKI, we give methods using different techniques their own name so they are easily distinguishable. We refer to the techniques listed in section 4.3.3. All methods are initialized in the same way (with the prior constructed based on the model) and all use mini-batching. We refer to the forward Euler discretization of equation (13) as EKI and the momentum discretization, presented in section 4.2.1, of equation (13) as MEKI. When randomizing around the mean at the end of each epoch, we refer to the method as EKI(R). When randomizing the momenta at each step, we refer to the method as MEKI(R). Similarly, we call momentum SGD, MSGD. All methods use the time step described in section 4.3.3 with hyper-parameters $h_0 = 2$ and $\epsilon = 0.5$ fixed. For any classification problem (except the voting records data set), all methods use the cross-entropy loss whose gradient is implemented with a slight correction for numerical stability. Namely, in the case of a single data point, we implement

$$(\nabla_{y'} \mathcal{L}(\mathcal{G}(u), y))_k = -\frac{y_k}{(\mathcal{G}(u))_k + \delta}$$

Dense Neural Networks		
Name	Architecture	Parameters
DNN 1	784-10	7,850
DNN 2	784-100-10	79,510
DNN 3	784-300-100-10	266,610
DNN 4	784-500-300-100-10	573,910

Figure 4. Architectures of the four dense neural networks considered. All networks use a softmax thresholding and a ReLU nonlinearity.

where the constant $\delta := 0.005$ is fixed for all our numerical experiments. Otherwise the mean squared-error loss is used. All implementations are done using the PyTorch framework [59] on a single machine with an NVIDIA GTX 1080 Ti GPU.

5.4. Supervised learning

5.4.1. Dense neural networks. In this section, we benchmark all of our proposed methods on the MNIST problem using four dense neural networks of increasing complexity. The four network architectures are outlined in figure 4. This will allow us to compare the methods and pick a front runner for later experiments. Furthermore we address scalability by finding the minimum number of ensemble members required to reach a certain accuracy on a dataset (standard set by SGD) for networks with increasing number of parameters. These experiments are performed with a two-layer dense network on MNIST and FashionMNIST. Lastly, we train a dense network with Heaviside activations (impossible with SGD) on FashionMNIST and compare to the equivalent ReLU network.

We fix the ensemble size of all methods to $J = 2000$ and the batch size to 600. SGD uses a learning rate of 0.1 and all momentum methods use the constant $\lambda = 0.9$. Figure 5 shows the final test accuracies for all methods while figure 6 shows the accuracies at the end of each epoch. Due to memory constrains, we do not implement MEKI for DNN-(3,4). In general momentum SGD performs best, but EKI(R) trails closely. The momentum EKI methods have good initial performance but saturate. We make this clearer in a later experiment. Overall, we see that for networks with a relatively small number of parameters all EKI methods are comparable to SGD. However with a large number of parameters, randomization is needed. This effect is particularly dominant when the ensemble size is relatively small; as we later show, larger ensemble sizes can perform significantly better.

Figure 7 shows the test accuracies for each of the particles when using EKI on DNN-(1,2). We see that, the mean particle achieves roughly the average of the spread, as previously discussed. Our choice to use it as the final parameter estimate is simply for convenience. One may use all the particles in a carefully weighted scheme as an ensemble of networks and possibly achieve better results. Having many parameter estimates may also be advantageous when trying to avoid adversarial examples [23]. We leave these considerations to future work.

To better illustrate the effect of the ensemble size, we compare all EKI methods on DNN 2 with an ensemble size of $J = 6000$. The accuracies are shown in figure 9. We again observe that the momentum methods perform very well initially, but fall off with more training. This effect could be related to the specific time discretization method we use, but needs to be studied further theoretically and we leave this for future work. Note that with a larger ensemble, EKI is now comparable to SGD pointing out that remaining in the subspace spanned by the initial ensemble is a bottle neck for this method. On the other hand, when we randomize, the ensemble size is no longer so relevant. EKI(R) performs almost identically with 2000 and

	DNN 1	DNN 2	DNN 3	DNN 4
SGD	0.9199	0.9735	0.9798	0.9818
MSGD	0.9257	**0.9807**	**0.9830**	**0.9840**
EKI	$\bar{u}$ 0.9092 $u^{(j^*)}$ 0.9114	$\bar{u}$ 0.9398 $u^{(j^*)}$ 0.9416	$\bar{u}$ 0.9424 $u^{(j^*)}$ 0.9432	$\bar{u}$ 0.9404 $u^{(j^*)}$ 0.9418
MEKI	$\bar{u}$ 0.9094 $u^{(j^*)}$ 0.9107	$\bar{u}$ 0.9320 $u^{(j^*)}$ 0.9332	n/a	n/a
EKI(R)	$\bar{u}$ 0.9252 $u^{(j^*)}$ **0.9260**	$\bar{u}$ 0.9721 $u^{(j^*)}$ 0.9695	$\bar{u}$ 0.9738 $u^{(j^*)}$ 0.9716	$\bar{u}$ 0.9741 $u^{(j^*)}$ 0.9691
MEKI(R)	$\bar{u}$ 0.9142 $u^{(j^*)}$ 0.9162	$\bar{u}$ 0.9509 $u^{(j^*)}$ 0.9511	n/a	n/a

Figure 5. Final test accuracies of six training methods on four dense neural networks, solving the MNIST classification problem. Each bold number is the maximum across the column. For each EKI method we report the accuracy of the mean particle $\bar{u}$ and of the best performing particle in the ensemble $u^{(j^*)}$.

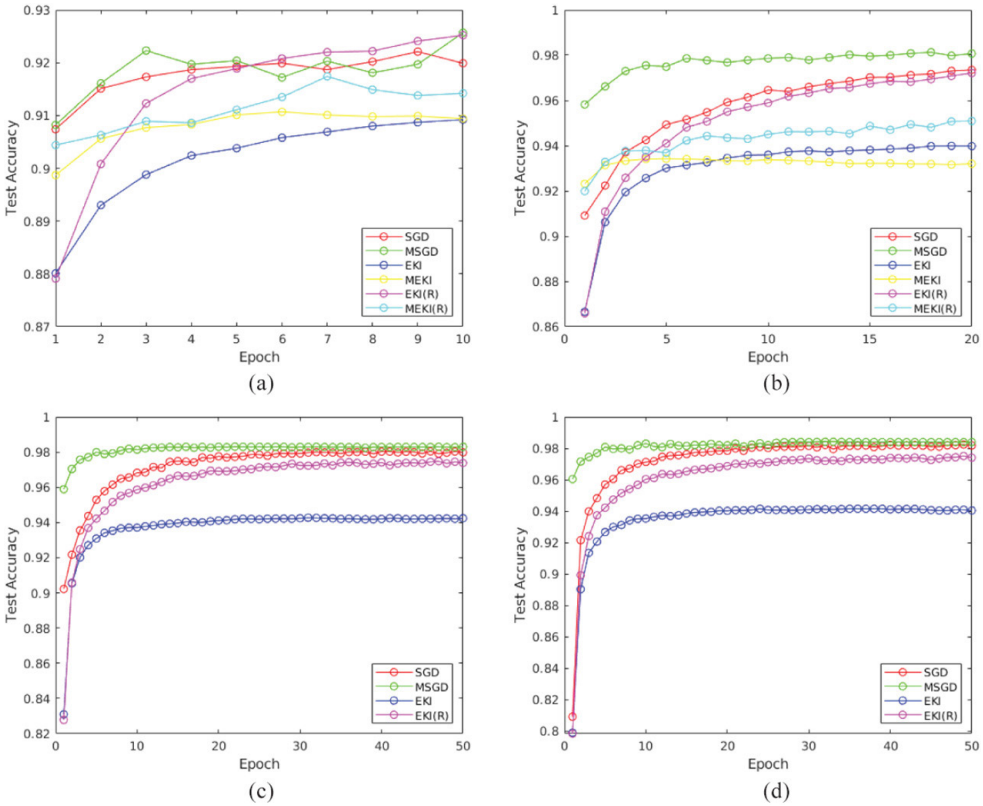

Figure 6. Test accuracies per epoch of six training methods on four dense neural networks, solving the MNIST classification problem. For each EKI method the accuracy of the mean particle $\bar{u}$ is shown. (a) DNN 1. (b) DNN 2. (c) DNN 3. (d) DNN 4.

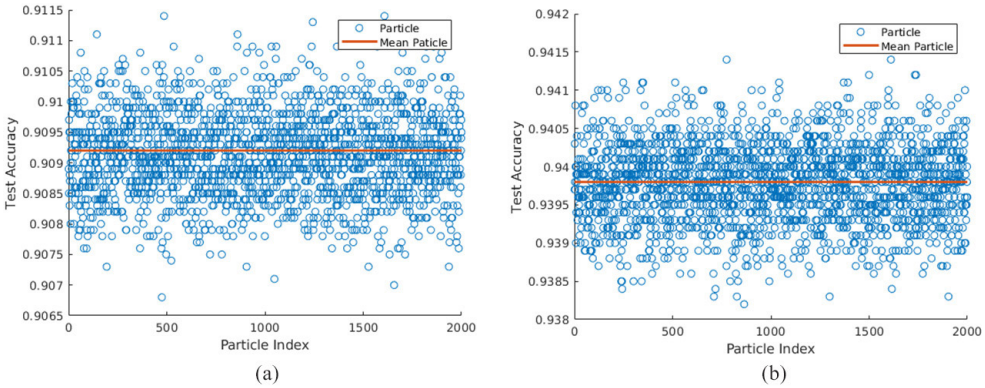

Figure 7. Particle accuracies of EKI on DNN-(1,2) compared to the accuracy of the mean particle $\bar{u}$. (a) DNN 1. (b) DNN 2.

with 6000 ensemble members. Finding it to be the best method for these tasks, all experiments hereafter, unless stated otherwise, use EKI(R).

To address scalability, we fix a network architecture (two-layer ReLU network) and find the smallest number of ensemble members J needed for EKI(R) to reach the maximum accuracy that can be achieved by this network given a fixed computational budget of 50 epochs. This accuracy is approximated via SGD on the same computational budget. We then increase the number of parameters in the network (keeping the architecture fixed) and repeat this experiment. The results are summarized in figure 10 for MNIST and FashionMNIST. We see that relatively few ensemble members are needed to reach the desired accuracy and the scaling with the number of parameters seems linear or sublinear. This is a promising indication that the EKI methodology can be scaled up to industrial-sized neural networks.

Lastly, since our method is derivative-free, we train a 784-100-10 network on FashionMNIST with Heaviside activation functions. This is impossible with gradient-based methods since the derivative of the Heaviside function is zero almost everywhere. This architecture is akin to Rosenblatt's original multi-layered perceptron [63]. We achieve 85% test set accuracy on this task which is comparable to the 87% achieved by the equivalent ReLU network. While our experiment is very simple, it demonstrates the possibility of being able to train non-differentiable neural networks which opens new avenues for network design that we hope will be explored in the future.

5.4.2. Convolutional neural networks For our experiments with CNN(s), we employ both MNIST and SVHN. Since MNIST is a fairly easy data set, we can use a simple architecture and still achieve almost perfect accuracy. We name the model CNN-MNIST and its specifics are given in the first column of figure 11. SGD uses a learning rate of 0.05 while momentum SGD uses 0.01 and a momentum factor of 0.9. EKI(R) has a fixed ensemble size of $J = 2000$. Figure 12 shows the results of training. We note that since CNN-MNIST uses ReLU and no batch normalization, SGD struggles to find a good descent direction in the first few epochs. EKI(R), on the other hand, does not have this issue and exhibits a smooth test accuracy curve that is consistent with all other experiments. In only 30 epochs, we are able to achieve almost perfect classification with EKI(R) slightly outperforming the SGD-based methods.

Recent work suggests that the effectiveness of batch normalization does not come from dealing with the internal covariate shift, but, in fact, comes from smoothing the loss surface [66]. The noisy gradient estimates in EKI can be interpreted as doing the same thing and

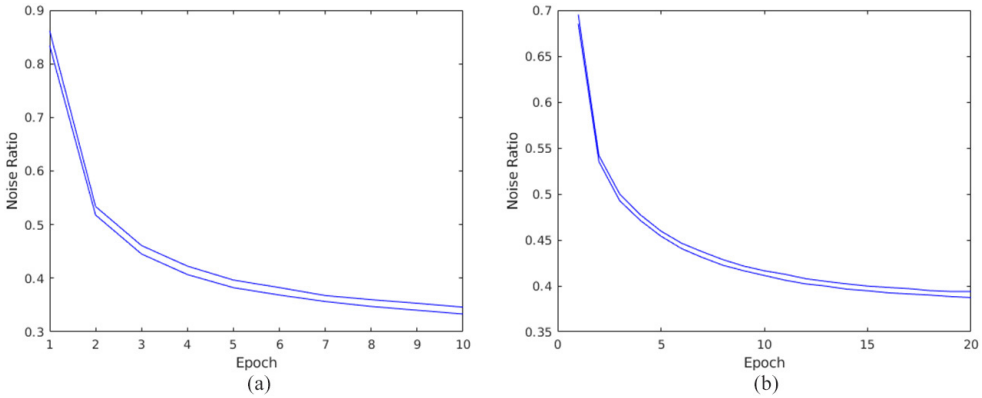

Figure 8. Spread of the noise ratio for EKI(R) on DNN-(1,2). At the end of every epoch, when the noise is added, the upper bound is computed as $\|\bar{u}\|_2 / \max_j \|\eta^{(j)}\|_2$. The lower bound is computed analogously. (a) DNN 1. (b) DNN 2.

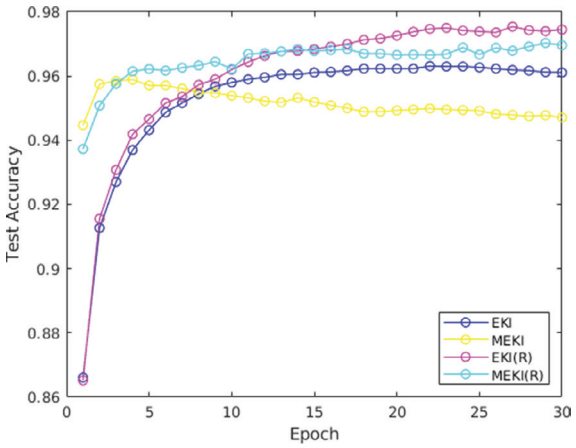

	First	Final
EKI	0.8661	0.9611
MEKI	**0.9447**	0.9471
EKI(R)	0.8652	**0.9745**
MEKI(R)	0.9373	0.9696

Figure 9. Comparison of the test accuracies of four EKI methods on DNN 2 with ensemble size $J = 6000$.

is perhaps the reason we see smoother test accuracy curves. The contemporaneous work of Haber *et al* [26] further supports this point of view.

Next we experiment on the SVHN data set with three CNN(s) of increasing complexity. The architectures we use are inspired by those in [50], and are referred to as fit-nets because each layer is shallow (has a relatively small number of parameters), but the whole architecture is deep, reaching up to sixteen layers. The details for the models dubbed CNN-(1,2,3) are given in figure 11. Such models are known to be difficult to train; for this reason, the papers [50, 62] present special initialization strategies to deal with the model complexities. We find that when using the SELU nonlinearity and no batch normalization, simple Xavier initialization works just as well. The results of training are presented in figure 12. We benchmark only against momentum SGD as all previous experiments show it performs better than vanilla SGD. The method uses a learning rate of 0.01 and a momentum factor of 0.9. EKI(R) starts with $J = 200$ ensemble members and expands by 200 at end the of each epoch until reaching a final ensemble of $J = 5000$. For CNN-3, memory constraints allowed us to only expand up

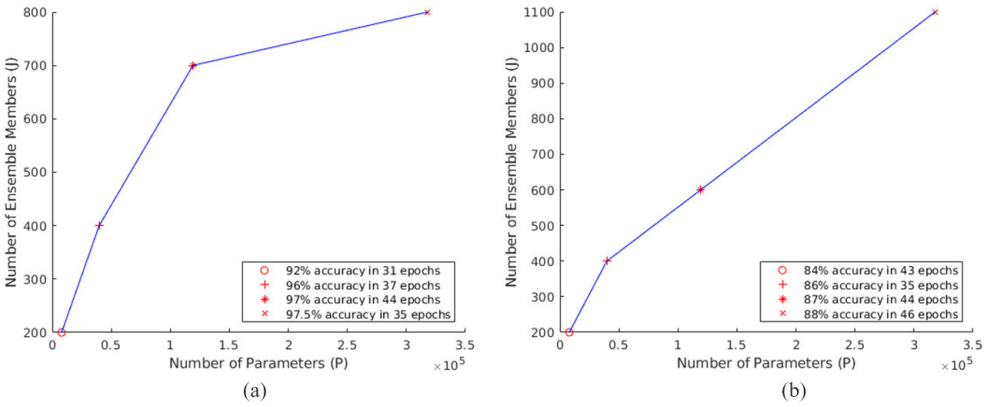

Figure 10. Minimum number of ensemble members needed to reach network capacity for a two-layer ReLU network within 50 epochs on MNIST and FashionMNIST. We increase the number of parameters in the first hidden layer and show the minimum J as a function of P. (a) MNIST. (b) FashionMNIST.

a final size of $J = 2800$. All methods use a batch size of 500. We see that, in all three cases, EKI(R) and momentum SGD perform almost identically with EKI(R) slightly outperforming on CNN-(1,2), but falling off on CNN-3. This is likely due to the fact that CNN-3 has a large number of parameters and we were not able to provide a large enough ensemble size. This issue can be dealt with via parallelization by splitting the ensemble among the memory banks of separate processing units. We leave this consideration to future work.

5.4.3. Recurrent neural networks. For the classification task using a recurrent neural network, we return to the MNIST data set. Since recurrent networks work on time series data, we split each image along its rows, making a 28-dimensional time sequence with 28 entries, considering time going down from the top to the bottom of the image. More complex strategies have been explored in [80]. We use a two-layer recurrent network with 32 hidden units and a $\tanh$ nonlinearity. Softmax thresholding is applied and the initial hidden state is always taken to be 0.

We train with a batch size of 600 and SGD uses a learning rate of 0.05. EKI(R) starts with an ensemble size of $J = 1000$ and expands by 1000 at the end of every epoch until $J = 4000$ is reached. Figure 13 shows the result of training. EKI(R) performs significantly better than SGD and appears more reliable, overall, for this task.

5.5. Semi-supervised learning

We proceed as in the construction of example 2.2, using the voting records data set. For the affinity measure we pick [7, 83]

$$\eta(x, y) = \exp\left(-\frac{\|x - y\|_2^2}{2(1.25)^2}\right)$$

and construct the graph Laplacian $\mathsf{L}(\mathsf{x})$. Its spectrum is shown in figure 3. Further we let $\tau = 0$ and $\alpha = 1$, hence the prior covariance $C = (\mathsf{L}(\mathsf{x}))^{-1}$ is defined only on the subspace orthogonal to the first eigenvector of $\mathsf{L}(\mathsf{x})$. The most naive clustering algorithm that uses a graph Laplacian simply thresholds the eigenvector of $\mathsf{L}(\mathsf{x})$ that corresponds to the smalled

Convolutional Neural Networks			
CNN-MNIST	CNN-1	CNN-2	CNN-3
Conv 16x3x3	Conv 16x3x3	Conv 16x3x3	Conv 16x3x3
Conv 16x3x3	Conv 16x3x3	Conv 16x3x3	Conv 16x3x3
		Conv 16x3x3	Conv 32x3x3
			Conv 32x3x3
			Conv 32x3x3
MaxPool 4x4 ($s = 2$)	MaxPool 2x2	MaxPool 2x2	MaxPool 2x2
Conv 16x3x3	Conv 16x3x3	Conv 32x3x3	Conv 48x3x3
Conv 16x3x3	Conv 16x3x3	Conv 32x3x3	Conv 48x3x3
		Conv 32x3x3	Conv 48x3x3
			Conv 48x3x3
			Conv 48x3x3
MaxPool 4x4 ($s = 2$)	MaxPool 2x2	MaxPool 2x2	MaxPool 2x2
Conv 12x3x3	Conv 32x3x3	Conv 48x3x3	Conv 64x3x3
Conv 12x3x3	Conv 32x3x3	Conv 48x3x3	Conv 64x3x3
		Conv 64x3x3	Conv 96x3x3
			Conv 96x3x3
			Conv 96x3x3
MaxPool 2x2	MaxPool 8x8	MaxPool 8x8	MaxPool 8x8
FC-10	FC-500	FC-500	FC-500
	FC-10	FC-10	FC-10

Figure 11. Architectures of 4 convolutional neural networks with 6, 7, 10, 16 layers respectively from left to right. All convolutions use a padding of 1, making them dimension preserving since all kernel sizes are 3x3. CNN-MNIST is evaluated on the MNIST dataset and uses the ReLU nonlinearity. CNN-(1,2,3) are evaluated on the SVHN dataset and use the SELU nonlinearity. The convention $s = 2$ refers to the stride of the max-pooling operation namely $\alpha = \beta = 2$. All networks use a softmax thresholding.

non-zero eigenvalue (called the Fiedler vector) [79]. Its accuracy is shown in figure 14. We found the best performing EKI method for this problem to simply be the vanilla version of the method i.e. no randomization or momentum. We use $J = 1000$ ensemble members drawn from the prior and the mean squared-error loss. Its performance is only slightly better than the Fiedler vector as the particles quickly collapse to something close to the Fiedler vector. This is likely due to the fact that the initial ensemble is an i.i.d. sequence drawn from the prior hence EKI converges to a solution in the subspace orthogonal to the first eigenvector of $\mathsf{L}(\mathsf{x})$ which is close to the Fiedler vector, especially if the weights and other attendant hyper-parameters have been chosen so that the Fielder vector already classifies the labeled nodes correctly. On the other hand, the MCMC method detailed in [7] can explore outside of this subspace and achieve much better results. We note, however, that EKI is significantly cheaper and faster than MCMC and thus could be applied to much larger problems where MCMC is not computationally feasible.

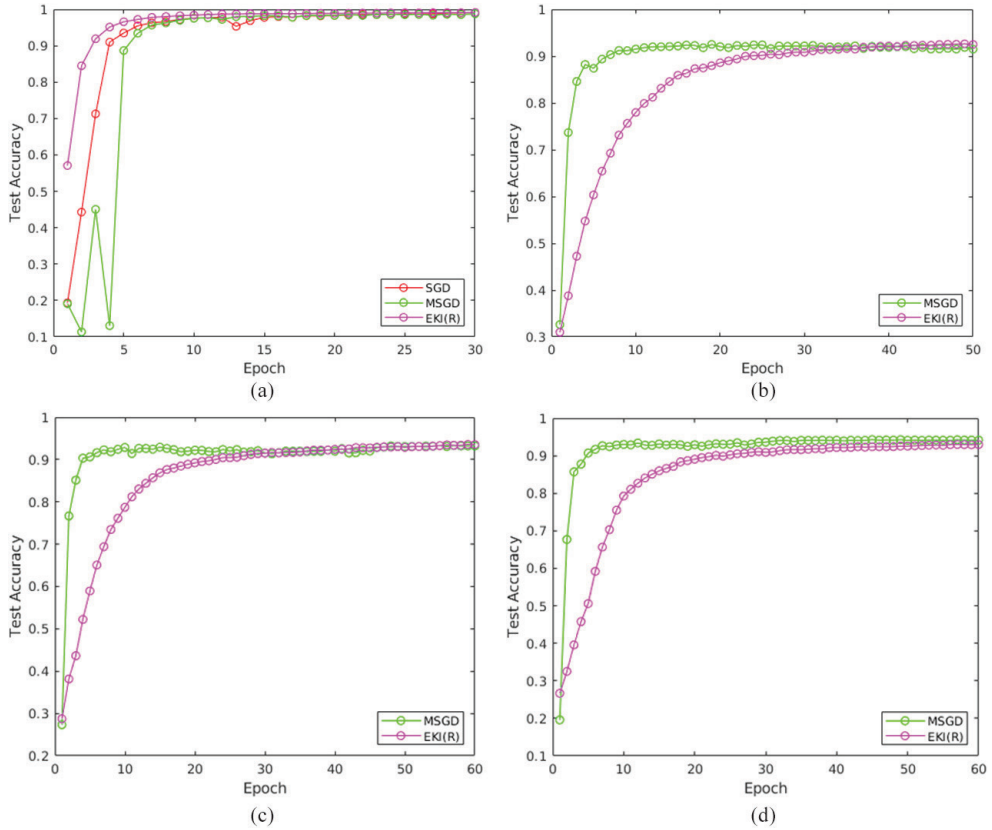

	CNN-MNIST		CNN-1		CNN-2		CNN-3	
	First	Final	First	Final	First	Final	First	Final
SGD	0.1936	0.9878	n/a	n/a	n/a	n/a	n/a	n/a
MSGD	0.1911	0.9880	**0.3263**	0.9150	0.2734	0.9324	0.1959	**0.9414**
EKI(R)	**0.5708**	**0.9912**	0.3100	**0.9249**	**0.2874**	**0.9353**	**0.2668**	0.9299

Figure 12. Comparison of the test accuracies of SGD and EKI(R) on four convolutional neural networks. SGD(M) refers to momentum SGD. CNN-MNIST is trained on the MNIST data set, while CNN-(1,2,3) are trained on the SVHN data set. (a) CNN-MNIST. (b) CNN-1. (c) CNN-2. (d) CNN-3.

5.6. Online learning

We now consider two online learning problems using a recurrent neural network. We employ two univariate time-series data sets: minimum daily temperatures in Melbourne, and the monthly number of sunspots observed from Zürich. For both, we use a single layer recurrent network with 32 hidden units and the tanh nonlinearity. The output is not thresholded i.e. $S = id$. At the initial time, we set the hidden state to zero then use the hidden state computed in the previous step to initialize for the current step. This is an online problem as our algorithm only sees one data-label pair at a time. For OGD, we use a learning rate of 0.001 while, for EKI, we use $J = 12$ ensemble members. Figure 15 shows the results of training as well as how well each of the trained model fits the test data. Notice that EKI converges much more quickly and to a slightly better solution than OGD in both cases. Furthermore, the model learned by

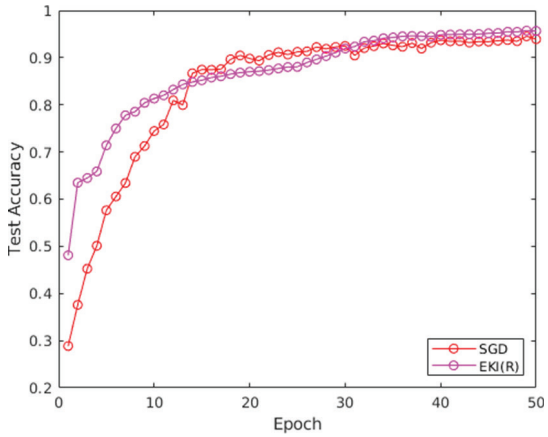

	First	Final
SGD	0.2825	0.9391
EKI(R)	**0.4810**	**0.9566**

Figure 13. Comparison of the test accuracies of EKI(R) and SGD on the MNIST data set with a two layer recurrent neural network.

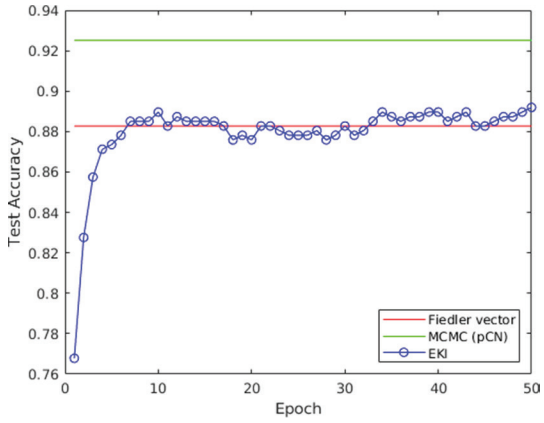

	Accuracy
Fiedler vector	0.8828
MCMC (pCN)	**0.9252**
EKI	0.8920

Figure 14. Comparison of the test accuracies of two semi-supervised learning algorithms to EKI on the voting records data set.

EKI is able to better capture small scale oscillations. These are very promising results for the application of EKI to harder RNN problems.

Finally we consider an online version of the classification problem. We train a CNN (using the architecture of CNN-MNIST given in figure 11) on MNIST and FashionMNIST for using only 10 training examples from each data set. The performance of this network on the test set is taken as a baseline. We then feed in 2000 examples from the training set sequentially one at a time (equivalent to a batch size of one) and update our model with OGD and EKI ($J = 2000$), comparing their performance in figure 16. We see that the two methods perform similarly, with EKI(R) trailing slightly behind in accuracy but having an overall lower variance. These results also confirm our intuition that EKI may be viewed as approximating gradient decent.

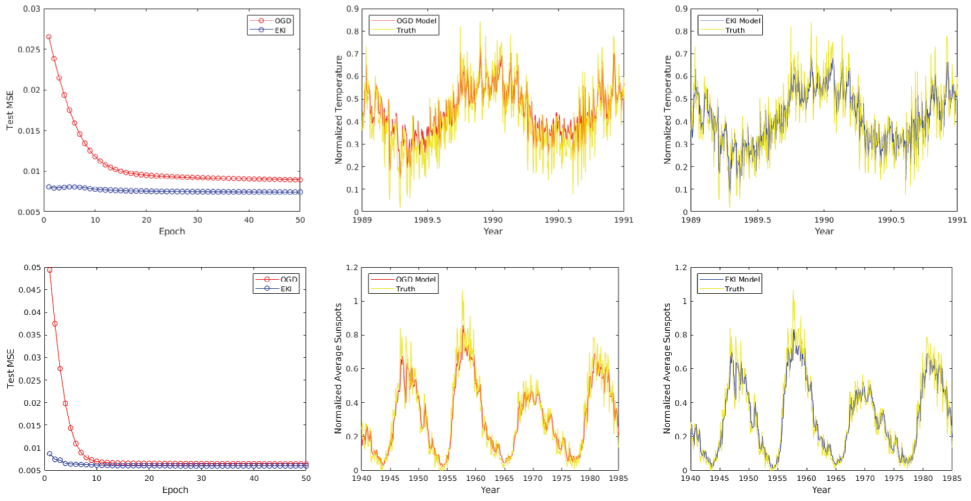

	Melbourne Temperatures		Zürich Sunspots	
	First	Final	First	Final
OGD	2.653×10^{-2}	8.954×10^{-3}	4.939×10^{-2}	6.480×10^{-3}
EKI	$\mathbf{8.086 \times 10^{-3}}$	$\mathbf{7.448 \times 10^{-3}}$	$\mathbf{8.671 \times 10^{-3}}$	$\mathbf{6.006 \times 10^{-3}}$

Figure 15. Comparison of OGD and EKI on two online learning tasks with a recurrent neural network. The top row shows the minimum daily temperatures in Melbourne data set, while the bottom shows the number of sunspots observed each month from Zürich data set.

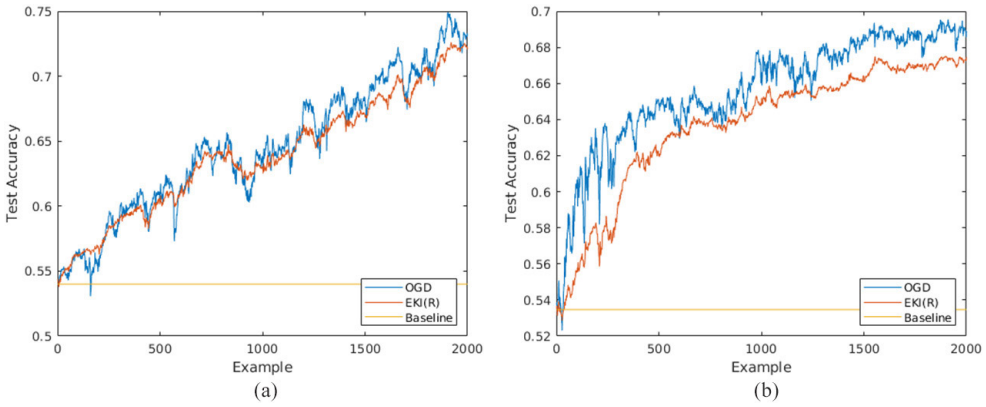

Figure 16. Comparison of OGD and EKI on the online classification task with MNIST and FashionMNIST. (a) MNIST. (b) FashionMNIST.

6. Conclusion and future directions

We have demonstrated that many machine learning problems can easily fit into the unified framework of Bayesian inverse problems. Within this framework, we apply ensemble Kalman inversion methods, for which we suggest suitable modifications, to tackle machine learning

tasks. Our numerical experiments suggest a wide applicability and competitiveness against the state-of-the-art for our schemes. The following directions for future research arise naturally from our work:

- Theoretical analysis of the momentum and general loss EKI methods as well as their possible application to physical inverse problems.
- GPU parallelization of EKI methods and its application to large scale machine learning tasks.
- Application of EKI methods to more difficult recurrent neural network problems as well as problems in reinforcement learning.
- Use of the entire ensemble of particle estimates to improve accuracy, to perform dimension reduction and possibly to combat adversarial examples.
- The development of Bayesian techniques to quantify uncertainty in trained neural networks.
- The use of ensemble methods in other momentum based algorithms such as Hamiltonian Monte Carlo.

Acknowledgments

Both authors are supported, in part, by the US National Science Foundation (NSF) grant DMS 1818977, the US Office of Naval Research (ONR) grant N00014-17-1-2079, and the US Army Research Office (ARO) grant W911NF-12-2-0022. The authors would also like to thank the anonymous reviewers for their many insightful comments.

ORCID iDs

Nikola B Kovachki https://orcid.org/0000-0002-3650-2972

References

[1] Allen-Zhu Z, Li Y and Song Z 2018 A convergence theory for deep learning via over-parameterization *CoRR* (arXiv:1811.03962)
[2] Andrews D and Herzberg A 1985 *Data: a Collection of Problems from Many Fields for the Student and Research Worker* (*Springer Series in Statistics* (New York: Springer)
[3] Bach F and Moulines E 2013 Non-strongly-convex smooth stochastic approximation with convergence rate o (1/n) *Advances in Neural Information Processing Systems* pp 773–81
[4] Bengio Y, Boulanger-lew N, Pascanu R and Montreal U 2013 Advances in optimizing recurrent networks *IEEE Int. Conf. on in Acoustics, Speech and Signal Processing*
[5] Bergemann K and Reich S 2010 A mollified ensemble Kalman filter *Q. J. R. Meteorol. Soc.* **136** 1636–43
[6] Bertozzi A and Flenner A 2012 Diffuse interface models on graphs for classification of high dimensional data *Multiscale Model. Simul.* **10** 1090–118
[7] Bertozzi A L, Luo X, Stuart A M and Zygalakis K C 2018 SIAM/ASA *J. Uncertainty Quantifi.* **6** 568–95
[8] Binkowski M, Marti G and Donnat P 2017 Autoregressive convolutional neural networks for asynchronous time series *CoRR* (arXiv:1703.04122)
[9] Boser B E, Guyon I M and Vapnik V N 1992 A training algorithm for optimal margin classifiers *Proc. of the 5th Annual Workshop on Computational Learning Theory* (New York, NY: ACM) pp 144–52

[10] Candes E J and Tao T 2006 Near-optimal signal recovery from random projections: universal encoding strategies? *IEEE Trans. Inf. Theor.* **52** 5406–25
[11] Carreira-Perpinan M and Wang W 2014 Distributed optimization of deeply nested systems ed S Kaski and J Corander *Proc. of the 17th Int. Conf. on Artificial Intelligence and Statistics* (*Proc. of Machine Learning Research* vol 33) (Reykjavik, Iceland) pp 10–9
[12] Chaudhari P, Choromanska A, Soatto S, LeCun Y, Baldassi C, Borgs C, Chayes J T, Sagun L and Zecchina R 2016 Entropy-sgd: biasing gradient descent into wide valleys *CoRR* (arXiv:1611.01838)
[13] Chaudhari P and Soatto S 2017 Stochastic gradient descent performs variational inference, converges to limit cycles for deep networks *CoRR* (arXiv:1710.11029)
[14] De Vito E, Rosasco L, Caponnetto A, De Giovannini U and Odone F 2005 Learning from examples as an inverse problem *J. Mach. Learn. Res.* **6**
[15] Dieuleveut A *et al* 2016 Nonparametric stochastic approximation with large step-sizes *Ann. Stat.* **44** 1363–99
[16] Duchi J, Hazan E and Singer Y 2011 Adaptive subgradient methods for online learning and stochastic optimization *J. Mach. Learn. Res.* **12** 2121–59
[17] Dunlop M 2017 private communication
[18] Evensen G 2003 The ensemble Kalman filter: theoretical formulation and practical implementation *Ocean Dyn.* **53** 343–67
[19] Ernst O G, Sprungk B and Starkloff H J 2015 Analysis of the ensemble and polynomial chaos Kalman filters in bayesian inverse problems *J. Uncertainty Quantifi.* **3** 823–51
[20] Gil-Alana L 2006 Long memory behaviour in the daily maximum and minimum temperatures in melbourne, australia *Meteorol. Appl.* **11** 319–28
[21] Glorot X and Bengio Y 2010 Understanding the difficulty of training deep feedforward neural networks *Proc. of the Int. Conf. on Artificial Intelligence and Statistics* (Society for Artificial Intelligence and Statistics)
[22] Goodfellow I, Bengio Y and Courville A 2016 *Deep Learning* (Cambridge, MA: MIT Press)
[23] Goodfellow I, Shlens J and Szegedy C 2015 Explaining and harnessing adversarial examples *Int. Conf. on Learning Representations*
[24] Graham B 2014 Fractional max-pooling *CoRR* (arXiv:1412.6071)
[25] Gulcehre C, Cho K, Pascanu R and Bengio Y 2014 Learned-norm pooling for deep feedforward and recurrent neural networks *Proc. of the European Conf. on Machine Learning and Knowledge Discovery in Databases* vol 8724 (Berlin: Springer) pp 530–46
[26] Haber E, Lucka F and Ruthotto L 2018 Never look back—a modified enkf method and its application to the training of neural networks without back propagation *CoRR* (arXiv:1805.08034)
[27] Haykin S S 2001 *Kalman Filtering and Neural Networks* (New York: Wiley)
[28] He K, Zhang X, Ren S and Sun J 2014 Spatial pyramid pooling in deep convolutional networks for visual recognition *Computer Vision—ECCV 2014* ed D Fleet *et al* (Cham: Springer) pp 346–61
[29] Hinton G and Salakhutdinov R 2006 Reducing the dimensionality of data with neural networks *Science* **313** 504–7
[30] Hoerl A E and Kennard R W 1970 Ridge regression: biased estimation for nonorthogonal problems *Technometrics* **12** 55–67
[31] Hornik K 1991 Approximation capabilities of multilayer feedforward networks *Neural Netw.* **4** 251–7
[32] Houtekamer P, He B and Mitchell H L 2014 Parallel implementation of an ensemble Kalman filter *Mon. Wea. Rev.* **142** 1163–82
[33] Iglesias M, Lu Y and Stuart A 2016 A bayesian level set method for geometric inverse problems *Interfaces Free Boundaries* **18** 181–217
[34] Iglesias M A, Law K J H and Stuart A M 2013 Ensemble Kalman methods for inverse problems *Inverse Problems* **29** 045001
[35] Jordan M 2017 On gradient-based optimization: accelerated, distributed, asynchronous and stochastic *ACM SIGMETRICS Performance Evaluation Review* vol 45 (ACM) p 58
[36] Bergemann K and Reich S 2010 A localization technique for ensemble Kalman filters *Q. J. R. Meteorol. Soc.* **136** 701–7
[37] Kiefer J and Wolfowitz J 1952 Stochastic estimation of the maximum of a regression function *Ann. Math. Stat.* **23** 462–6
[38] Kingma D P and Ba J 2014 Adam: a method for stochastic optimization *CoRR* (arXiv:1412.6980)

[39] Klambauer G, Unterthiner T, Mayr A and Hochreiter S 2017 Self-normalizing neural networks *Advances in Neural Information Processing Systems 30* ed I Guyon *et al* (Curran Associates and Inc.) pp 971–80
[40] Kovachki N B and Stuart A M 2019 Analysis of momentum methods preprint
[41] Krizhevsky A, Sutskever I and Hinton G E 2012 Imagenet classification with deep convolutional neural networks *Advances in Neural Information Processing Systems 25* ed F Pereira *et al* (Curran Associates and Inc.) pp 1097–105
[42] Law K, Stuart A and Zygalakis K 2015 *Data Assimilation: a Mathematical Introduction* (*Texts in Applied Mathematics* vol 62) (Cham: Springer)
[43] LeCun Y, Bengio Y and Hinton G E 2015 Deep learning *Nature* **521** 436–44
[44] Lecun Y, Bottou L, Bengio Y and Haffner P 1998 Gradient-based learning applied to document recognition *Proc. of the IEEE* pp 2278–324
[45] LeCun Y and Cortes C 2010 MNIST handwritten digit database
[46] Lee J D, Simchowitz M, Jordan M I and Recht B 2016 Gradient descent only converges to minimizers *Conf. on Learning Theory* pp 1246–57
[47] Litjens G J S, Kooi T, Bejnordi B E, Setio A A A, Ciompi F, Ghafoorian M, van der Laak J A W M, van Ginneken B and Sánchez C I 2017 A survey on deep learning in medical image analysis *CoRR* (arXiv:1702.05747)
[48] Manning C D and Schütze H 1999 *Foundations of Statistical Natural Language Processing* (Cambridge, MA: MIT Press)
[49] McCullagh P and Nelder J 1989 *Generalized Linear Models, Second Edition* (*Chapman and Hall/CRC Monographs on Statistics and Applied Probability Series*) (London: Chapman and Hall)
[50] Mishkin D and Matas J 2015 All you need is a good init *CoRR* (arXiv:1511.06422)
[51] Murphy K P 2012 *Machine Learning: a Probabilistic Perspective* (Cambridge, MA: MIT Press)
[52] Nagi J, Ducatelle F, Caro G A D, Ciresan D, Meier U, Giusti A, Nagi F, Schmidhuber J and Gambardella L M 2011 Max-pooling convolutional neural networks for vision-based hand gesture recognition
[53] Nair V and Hinton G E 2010 Rectified linear units improve restricted boltzmann machines *Proc. of the 27th Int. Conf. on Int. Conf. on Machine Learning* (Omnipress) pp 807–14
[54] Nesterov Y 1983 A method of solving a convex programming problem with convergence rate o(1/k2) *Sov. Math. Dokl.* **27** 372–6
[55] Netzer Y, Wang T, Coates A, Bissacco A, Wu B and Ng A Y 2011 Reading digits in natural images with unsupervised feature learning
[56] Niño E D, Sandu A and Deng X 2016 A parallel implementation of the ensemble Kalman filter based on modified cholesky decomposition *CoRR* (arXiv:1606.00807)
[57] Nino-Ruiz E D and Sandu A 2015 An efficient parallel implementation of the ensemble Kalman filter based on shrinkage covariance matrix estimation *Proc. of the 2015 IEEE 22nd Int. Conf. on High Performance Computing Workshops* (Washington, DC: IEEE Computer Society) p 54
[58] Pascanu R, Mikolov T and Bengio Y 2013 On the difficulty of training recurrent neural networks *Proc. of the 30th Int. Conf. on Int. Conf. on Machine Learning* vol 28 pp III-1310–8
[59] Paszke A, Gross S, Chintala S, Chanan G, Yang E, DeVito Z, Lin Z, Desmaison A, Antiga L and Lerer A 2017 Automatic differentiation in pytorch NIPS-W
[60] Rasmussen C E and Williams C K 2006 *Gaussian Process for Machine Learning* (Cambridge, MA: MIT Press)
[61] Robbins H and Monro S 1951 A stochastic approximation method *Ann. Math. Stat.* **22** 400–7
[62] Romero A, Ballas N, Kahou S E, Chassang A, Gatta C and Bengio Y 2015 Fitnets: hints for thin deep nets *Proc. of ICLR*
[63] Rosenblatt F 1958 The perceptron: a probabilistic model for information storage and organization in the brain *Psychol. Rev.* **65** 386–408
[64] Ruck D W, Rogers S K, Kabrisky M, Oxley M E and Suter B W 1990 The multilayer perceptron as an approximation to a bayes optimal discriminant function *IEEE Trans. Neural Netw.* **1** 296–8
[65] Rumelhart D E, Hinton G E and Williams R J 1988 Chapter: learning representations by back-propagating errors *Neurocomputing: Foundations of Research* (Cambridge, MA: MIT Press) pp 696–9
[66] Santurkar S, Tsipras D, Ilyas A and Madry A 2018 How does batch normalization help optimization? (no, it is not about internal covariate shift) *CoRR* (arXiv:1805.11604)
[67] Schillings C and Stuart A M 2017 Analysis of the ensemble Kalman filter for inverse problems *SIAM J. Numer. Anal.* **55** 1264–90

[68] Schmidt M, Le Roux N and Bach F 2017 Minimizing finite sums with the stochastic average gradient *Math. Program.* **162** 83–112
[69] Stuart A and Humphries A R 1998 *Dynamical Systems and Numerical Analysis* vol 2 (Cambridge: Cambridge University Press)
[70] Su W, Boyd S and Candes E 2014 A differential equation for modeling nesterov's accelerated gradient method: theory, insights *Advances in Neural Information Processing Systems 27* ed Z Ghahramani *et al* (Curran Associates and Inc.) pp 2510–8
[71] Such F P, Madhavan V, Conti E, Lehman J, Stanley K O and Clune J 2017 Deep neuroevolution: genetic algorithms are a competitive alternative for training deep neural networks for reinforcement learning *CoRR* (arXiv:1712.06567)
[72] Sutskever I, Martens J, Dahl G and Hinton G 2013 On the importance of initialization and momentum in deep learning *Proc. of the 30th Int. Conf. on Int. Conf. on Machine Learning* vol 28
[73] Sutskever I, Vinyals O and Le Q V 2014 Sequence to sequence learning with neural networks *Proc. of the 27th Int. Conf. on Neural Information Processing Systems* vol 2 (Cambridge, MA: MIT Press) pp 3104–12
[74] Szegedy C, Zaremba W, Sutskever I, Bruna J, Erhan D, Goodfellow I and Fergus R 2014 Intriguing properties of neural networks *Int. Conf. on Learning Representations*
[75] Taylor G, Burmeister R, Xu Z, Singh B, Patel A and Goldstein T 2016 Training neural networks without gradients: a scalable admm approach *Proc. of the 33rd Int. Conf. on Int. Conf. on Machine Learning* vol 48 pp 2722–31
[76] Tsai Y H, Hamsici O C and Yang M H 2015 Adaptive region pooling for object detection *IEEE Conf. on Computer Vision and Pattern Recognition* pp 731–9
[77] Vapnik V N 1995 *The Nature of Statistical Learning Theory* (Berlin: Springer)
[78] Vogel C R 2002 *Computational Methods for Inverse Problems* (Philadelphia, PA: SIAM)
[79] von Luxburg U 2007 A tutorial on spectral clustering *Stat. Comput.* **17** 395–416
[80] Wang J, Yang Y, Mao J, Huang Z, Huang C and Xu W 2016 Cnn-rnn: a unified framework for multi-label image classification *IEEE Conf. on Computer Vision and Pattern Recognition* pp 2285–94
[81] Wilson A C, Roelofs R, Stern M, Srebro N and Recht B 2017 The marginal value of adaptive gradient methods in machine learning ed I Guyon *et al Advances in Neural Information Processing Systems 30* (Curran Associates and Inc.) pp 4148–58
[82] Xiao H, Rasul K and Vollgraf R 2017 Fashion-mnist: a novel image dataset for benchmarking machine learning algorithms *CoRR* (arXiv:1708.07747)
[83] Zelnik-manor L and Perona P 2005 Self-tuning spectral clustering *Advances in Neural Information Processing Systems 17* ed L K Saul *et al* (Cambridge, MA: MIT Press) pp 1601–8
[84] Zhang S, Choromanska A and LeCun Y 2015 Deep learning with elastic averaging sgd *Proc. of the 28th Int. Conf. on Neural Information Processing Systems* vol 1 (Cambridge, MA: MIT Press) pp 685–93